Response to Anonymous Referee #1

Yuzhe Wang

We would like to thank the anonymous referee #1 for giving constructive comments on our paper. We have responded each comment with great care. The original comments of the reviewer are given in italic, and our responses are given directly below in regular.

General comments

Although the graph are nicely prepared and the structure of the paper is clear, the too obvious similarities with Zhang et al. [2013] give the impression of reading exactly the same paper The only change is the way that thermal boundary condition are addressed which is not a real improvement. I suggest to explore the transient state using available meteorological data to distinct this new study from Zhang et al. [2013].

It's true both studies share a few of similarities. After the attempt of Zhang et al. (2013) on the East Rongbuk Glacier, Mt. Qomolangma (Everest), we've been curious about the thermo-mechanical features of other typical Tibetan mountain glaciers. Does the climate warming really have a great impact on these glaciers and how much are these impacts? The East Rongbuk Glacier is at the southern edge of Tibetan Plateau. The one we get interested this time, Laohugou Glacier No. 12, is, however, at the northeastern edge of Tibetan Plateau. Despite the big different locations and climate backgrounds, both glaciers have been taken as fully cold for quite a long time by our China glaciological community. We hope that, by using similar numerical techniques, we could possibly get some interesting findings that can guide us to a big picture of Tibetan glacier changes. For example, does this 2D flowband model really work for mountain valley glaciers (we can save a lot of field efforts and money if it or something similar works)? If yes, how much can we rely on it? if not, how can we improve it? But first we should test it at different locations. That's the main reason we use a similar model approach and study method to Zhang et al. (2013).

We agree that the past climate change may have a great influence on the glacier velocities and temperature field. The difference between our diagnostic model results and the observations can be either from the assumptions of the model physics or the transient state of glacier change. We really wish we could do the transient study for LHG12 (and the East Rongbuk Glacier). Despite some previous expeditions in 1970s and 1980s, there is very few long-term series of meteorological data available in this area. The glaciological station was established in 2008 and we do not have the radar gemotry data of 2008 either. Thus, our aim is to investigate the current thermo-mechanical state by neglecting the transient impacts. We know by doing this there will be some uncertainties in our model results. We assume the transient effect in past years is stable and our thermal steady-state assumption is effective. We believe that our thermal steady-state model can capture some characteristics of glacier behaviours within the range of historical changes, and that our conclusion that LHG12 is now polythermal should be robust. To be as cautious as we can, we avoid showing precise number of, like, temperate ice zone lengths and thickness in both the abstract and the conclusions.

The thermal surface boundary condition should be better addressed. As I said above, the 20-meter-deep temperature is representative of the climatic forcing on the glacier energy balance during the previous year only. Using this temperature as boundary condition of a steady state simulation will lead to a temperature field probably far from the reality. The authors should, at least, try to develop a parametrization that linked T_{sbc}, T_{air} and the ELA elevation based on the available observations on the glacier. I recommend to use in the ablation zone $T_{sbc} = T_{air} + constant$ and find the constant that allows to match the measured T_{20m} instead of using the approach of Wohlleben et al. [2009] which is very qualitative

As suggested by the reviewer, we now prescribe the T_{sbc} in the ablation area by a simple parameterization $T_{\mathrm{sbc}} = T_{\mathrm{air}} + c$, where c is a tuning parameter including the impacts of both the surface energy budget and the steady-state temperature Gilbert et al. (2010). We vary the values of c from 0 to 6 K (with a step-size of 0.2 K) and compare the modeled 20 m borehole temperatures with in-situ annual measurements at site 1 and 2 (Fig. 1). As shown in Fig. 1b (in manuscript), site 1 is located at the center of the confluence area where the convergent flow from the west branch joins the mainstream. Thus, at site 1 it is difficult to find a good c value that predicts close temperature comparisons to the observations. We therefore determine the c value (1.6 K) based on the fittings between the modeled and observed ice temperature data at site 2.

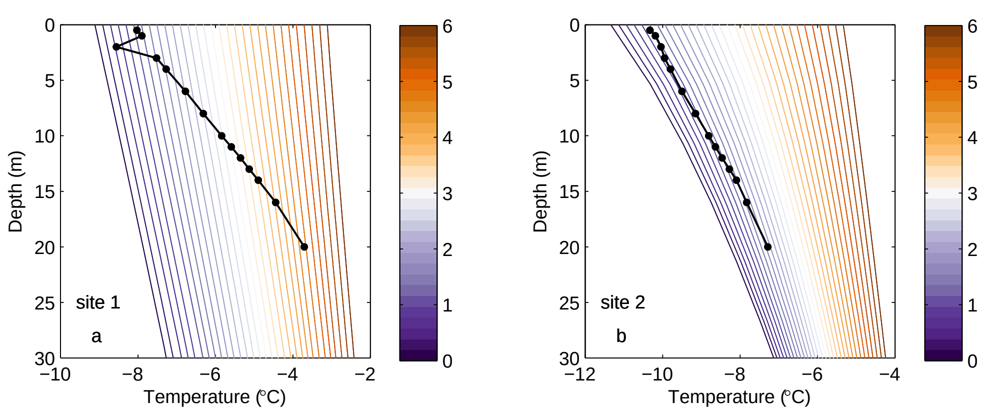

Figure 1: Sensicitity experiments of the tuning parameter c by comparing the measured (black dotted lines) and modeled (coloured lines) 20 m borehole temperatures at sites 1 (a) and 2 (b). The step-size of varying the c value is 0.2 K.

In addition, we also compare the differences between the new (E-new, (Gilbert et al., 2010)) and the old (E-old, (Wohlleben et al., 2009)) parameterizations of the thermal surface boundary conditions (Fig. 2). It shows that the two experiments produce very similar results in terms of modeled ice surface velocities, basal sliding velocities, temperate ice zones, and temperature profiles at the deep borehole (Fig. 2b, c, d). As can be expected, the modeled column mean and basal temperatures in the distance of km 5.0 – 9.1 demonstrate large differences due to the different parameterizaitions in the ablation area (Fig. 2a).

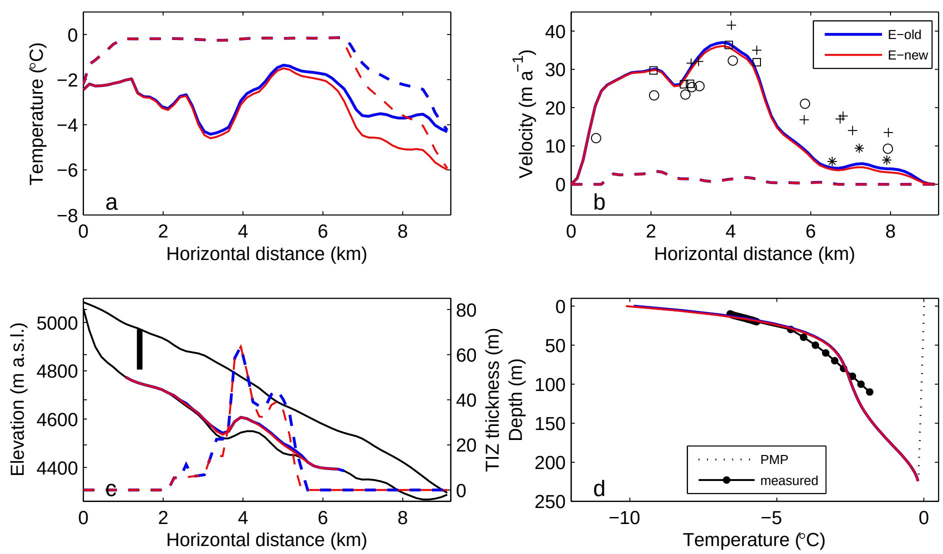

Figure 2: Modeled ice temperatures and velocities for experiments E-old (blue line) and E-new (red line). (a) Modeled column mean (solid lines) and basal (dashed lines) ice temperatures along the center flowline. (b) Modeled surface (solid lines) and basal (dashed lines) ice velocities along the CL. The symbols show the measured ice surface velocities same as in the manuscript. (c) Modeled CTS position (solid lines) and TIZ thickness (dashed lines). The black bar shows the location of the deep ice borehole. (d) Measured (dots) and modeled (coloured lines) ice temperature profiles for the deep borehole. The dotted line shows the pressure-melting point as a function of ice depth.

I don't see any dependence of the sliding law to temperature. The authors seem to assume that sliding only depend of the effective pressure which is assumed to be uniformly proportional to the hydrostatic pressure in their study. This is very disputable, modeling sliding in cold area is very unusual in glaciology Also, surface velocity measurement do not bring the evidence of sliding on this glacier. I think that removing sliding in the model still lead to modeled surface velocities under the measurements uncertainties (see next comment).

It's not true. The sliding events are certainly a result of the existence of temperate ice. At the ice-bed interface, we prescribe a non-slip boundary condition where ice is frozen to the bed (cold ice) and a Coulomb friction law where ice is temperate, i.e., the ice temperature reaches the local pressure-melting point. We have clarified this in p6–line9.

Uncertainty on the surface velocity should be indicated to be able to discuss about the goodness of the fit and comparing velocity measurements at different periods. Is the difference between winter, summer and annual mean velocities are really significant?

We agree the reviewer that the uncertainties of the ice velocity data are important for evaluating our model results. We estimate the data uncertainty below 1 m a^{-1}. But the stakes are not exactly located on the center flowline, which may also bring some unknown uncertainties. The summer (2008) and winter (2010) velocity data we have are not from a single year. They cannot be exactly compared. But from the only overlapped point we have (Fig. 3 in the manuscript), the difference between winter and summer values is non-negligible – it could be up to around 50%. We have added the uncertainties of GPS positioning and the calculated velocities in p3 – line23-24.

I note that the author have placed the ELA elevation to be able to "fit" their deep borehole data but is this ELA elevation really correspond to what is observed on the field?

The ELA was identified from the Landsat image on September 6, 2011, which is quite close the time (October 1–6, 2011) we drilled the borehole.

Specific comments

I think you could write "englacial" instead of "en-glacial" everywhere.

Changed.

P1 line 1: Remove first sentence

Removed.

P1 line 3: Mt Qilian Shan located in

Changed.

P1 line 6: match well (remove well before "but clearly")

Changed.

P1 line 7: "because the flow branch is ignored": this assertion is not really supported by anything in the paper and many other reason could be invoked

It's correct that the neglect of the flow branch may be one of many reasons. We have conducted two other experiments by increasing the glacier width as a proxy of convergent effects of the west branch and by adjusting the friction sliding parameters at the confluence area. We found that both basal sliding and convergent effect can largely influence the ice surface velocities in that area. We now add several sentences in p9–line3-10 and also include an additional figure (Fig. 9 in manuscipt)

P1 line 7: "agree closely" : I don't agree, this is not a close match

From our point of view, it's quite close, given the facts of the sparse observations and the simplified 2D model we use. But as the reviewer suggested, we now remove "closely".

P1 line 9: were highly: are highly

Corrected.

P1 - line 9: Remove (for example temperature)

Removed.

P1 line 10: I don't think we can speak of the "work of Wohlleben et al. [2009]" talking about the qualitative assumption made is this paper

P1 line 13-14: Like (...) LHG12: this is not true. Most important parameter are surface conditions including snow cover thickness and summer melting intensity.

We thank the reviewer for this comment. We now change the sentence as "strain heating is an important parameter controlling the englacial thermal structure in LHG12." .

P1 line 18-19: Sentence too long

Changed. Now the sentence becomes
"Located on the northeastern edge of the Tibetan Plateau (36 – 39 °N, 94 – 104 °E), Mt. Qilian Shan (MQS) develops 2051 glaciers covering an area of approximately 1057 km^2 with a total ice volume of approximately 50.5 km^3 (Guo et al., 2014, 2015). Meltwater from MQS glaciers is a very important water resource for the agricultural irrigation and socio-economic development of the oasis cities in northwestern China."

P2 - line 11-13: Bad example: what is the link with a full stokes model here?

This example was mainly for underlining the importance of temperate ice. But we agree with the reviewer. The sentence is now removed. Lines 10–13 have been changed to:
"The temperature distribution of a glacier primarily controls the ice flow rheology, englacial hydrology, and basal sliding conditions (Blatter and Hutter, 1991; Irvine-Fynn et al., 2011; Schäfer et al., 2014). A good understanding of the glacier thermal regime is important for predicting glacier response to climate change (Wilson et al., 2013; Gilbert et al., 2015), improving glacier hazard analysis (Gilbert et al., 2014a), and reconstructing past climate histories (Lüthi and Funk, 2001; Gilbert et al., 2010)."

P2 line 13: In addition = not appropriate here

This line has been changed as shown in above.

P2 - line 14: "can be strongly influenced": this is the main control!!

We have corrected it and add some corresponding references. Now it reads:

"The thermal regime of a glacier is mainly controlled by the surface thermal boundary conditions (e.g., Gilbert et al., 2014b; Meierbachtol et al., 2015). For example, near-surface warming from refreezing melt-water and cooling from the cold air of crevasses influence the thermal regimes of glaciers (Wilson and Flowers, 2013; Wilson et al., 2013; Gilbert et al., 2014a)."

P2 - line 22: remove "extremely"

We consider the LHG12 as an extremely continental-type glacier according to the classification of Shi and Liu (2000) who categorized the China glaciers into three types: the maritime (temperate) type, sub-continental (sub-polar) type and extremely continental (polar) type. We prefer to keep "extremely" as an identifier to the sub-continental type.

P3 line 12: explain why you are interested in parametrizing transverse profile?

The LHG12 is a valley glacier which is confined to channels with lateral drag exerted by the valley walls. As you all know, the lateral drag has a remarkable impact on glacier dynamics. To account for the lateral drag in a 2D ice flow model, we may either use a so-called "shape factor" proposed initially by Nye (1965) and impressed again recently by Adhikari and Marshall (2012) or make a parameterization based on glacier widths at all depths (Pimentel et al., 2010; Zhang et al., 2013). By parametering the transverse profile based on GPR measurements, we can derive the widths of glacier cross-sections and parameterize lateral drags at different depths (section 3.1). We now add an additional sentence for explanation in p3–line11-13.

P3 line 18 -29: Give uncertainty on the measurement

We have added a description of the uncertainties on the measurements.

"We measured the stake positions using a real-time kinematic (RTK) fixed solution by a South Lingrui S82 GPS system (Liu et al., 2011). The accuracy of the GPS positioning is an order of a few centimeters and the uncertainty of the calculated ice surface velocties is estimated to be less than 1 m a^{-1}."

P4 line 20-24: There is no interest to detail the shape of the profile in the active layer

We have deleted the description of temperature variations in the active layer.

P4 line 28-29: Give the assumption of the model

We now add the assumptions. “By assuming the vertical normal stress as hydrostatic and neglecting the bridging effects (Pattyn, 2002), the equation for momentum balance is given as”.

P5 equation 6: reference?

It’s (Pattyn, 2002). Now added.

P6 equation 10: value of Γ *is not discussed*

$\Gamma = 0.84 m_{\max}$. Now added.

P8 - line 12: The authors claim a close match between model and observations at 80-90 m depth in the deep borehole: this is the point where the two curves (data and model) are just crossing! This not shows a good agreement between data and measurement.

LHG12 is a very large valley glacier. Though a lot of field work have been taken on this glacier, the *in-situ* observations are still sparse and temporally discontinuous. This is also one of many reasons that we didn’t try 3D Stokes ice flow model. It’s true that there are still some obvious disagreements between modeling results and *in-situ* observations. But given these poorly datasets, we are actually quite happy about the curves. However, as the reviewer suggested, we have removed the word “close”.

P8 line 33: Is there moulin on this cold glacier?

Yes, we observed several moulins in the middle ablation area in 2009 and 2014.

P11 line 1-2: Remove sentence

Removed.

References

Adhikari, S. and Marshall, S. J.: Parameterization of lateral drag in flowline models of glacier dynamics, Journal of Glaciology, 58, 1119–1132, 2012.

Gilbert, A., Wagnon, P., Vincent, C., Ginot, P., and Funk, M.: Atmospheric warming at a high-elevation tropical site revealed by englacial temperatures at Illimani, Bolivia (6340 m above sea level, 16°S, 67°W), Journal of Geophysical Research, 115, D10 109, 2010.

Nye, J.: The flow of a glacier in a channel of rectangular, elliptic or parabolic cross-section, Journal of Glaciology, 5, 661–690, 1965.

Pattyn, F.: Transient glacier response with a higher-order numerical ice-flow model, Journal of Glaciology, 48, 467–477, 2002.

Pimentel, S., Flowers, G. E., and Schoof, C. G.: A hydrologically coupled higher-order flow-band model of ice dynamics with a Coulomb friction sliding law, Journal of Geophysical Research: Earth Surface, 115, 2010.

Shi, Y. and Liu, S.: Estimation on the response of glaciers in China to the global warming in the 21st century, Chinese Science Bulletin, 45, 668–672, 2000.

Wohlleben, T., Sharp, M., and Bush, A.: Factors influencing the basal temperatures of a High Arctic polythermal glacier, Annals of Glaciology, 50, 9–16, 2009.

Zhang, T., Xiao, C., Colgan, W., Qin, X., Du, W., Sun, W., Liu, Y., and Ding, M.: Observed and modelled ice temperature and velocity along the main flowline of East Rongbuk Glacier, Qomolangma (Mount Everest), Himalaya, Journal of Glaciology, 59, 438–448, 2013.

Response to Referee #2

Yuzhe Wang

We would like to thank Martin Lüthi for giving insightful and constructive comments on our paper; they were very helpful to improve our manuscript. Our responsees to all the comments are given below. The original comments of the reviewer are given in italic, and our responses are given directly below in regular.

Specific comments

Leave away colons (:) before equations, this is not usual in The Cryosphere.

We have deleted colons before equations and have reformulated the sentences if necessary.

You should decide on one version of English. Now there are "modeled" and "modelled" in the same sentence.

We now use "modeled" and "modeling" in the manuscript.

p1,1 "see" could be omitted

Changed. We have also removed "see" appeared in other similar case.

p3,11 also give the slope angle in degrees, i.e. 4.6°.

Changed.

p3,12 L is often used for the glacier length, y would be more common for a transverse coordinate.

We have changed the equation to $z = aW(z)^b$.

p3,19 also indicate distance from terminus, or along-profile

We have added the distance information. The sentence now reads:

"All stakes were located in the distance between km 0.6 – 7.9 along the CL (Fig. 3), spanning an elevation range of 4355 – 4990 m.a.s.l. (Fig. 1)."

p5,13 omit ":", maybe writing "following Flowers et al. (2011)"

The sentence has been reformulated to "we parameterize the lateral drag, σ'_{xy}, as a function of the flow-band half width, W, following Flowers et al. (2011)".

p5,16 "horizontal diffusion is parametrized by glacier width" is quite opaque. Please explain what you are doing, since this is not standard. This seems to be middle term in the parentheses, but it is not clear where this comes from. Does this somehow parametrize lateral diffusion (along the y-Axis)? But then, why would the longitudinal velocity gradient dT/dx play a role? Please explain this in detail (maybe in an appendix).
Overall, it seems advantageous to ignore heat flow in y-direction (i.e. leave away the problematic term in Equation (6), since nothing is known about the boundary conditions there.

We directly use the parameterization of heat diffusion in y from Pattyn (2002) (Equation (16)) therein). It's just a rough assumption. We didn't check with F. Pattyn for the details of the mathematical derivation. The thoughts behind it, by our understanding, are from (1) assuming $\partial T/\partial x$ has a linear relationship with $\partial T/\partial y$, $\partial T/\partial y = \partial W/\partial x \times \partial T/\partial x$; (2) assuming $\partial^2 T/\partial y^2 = 1/W \times \partial T/\partial y$.

As suggested by the reviewer, we now have removed the diffusion term in y. As shown below, this diffusion along y (E-yDiffu) has very limited impact on the model results, compared with the case without it (E-ref). Thus, we can indeed ignore this term in the 2D ice temperature model.

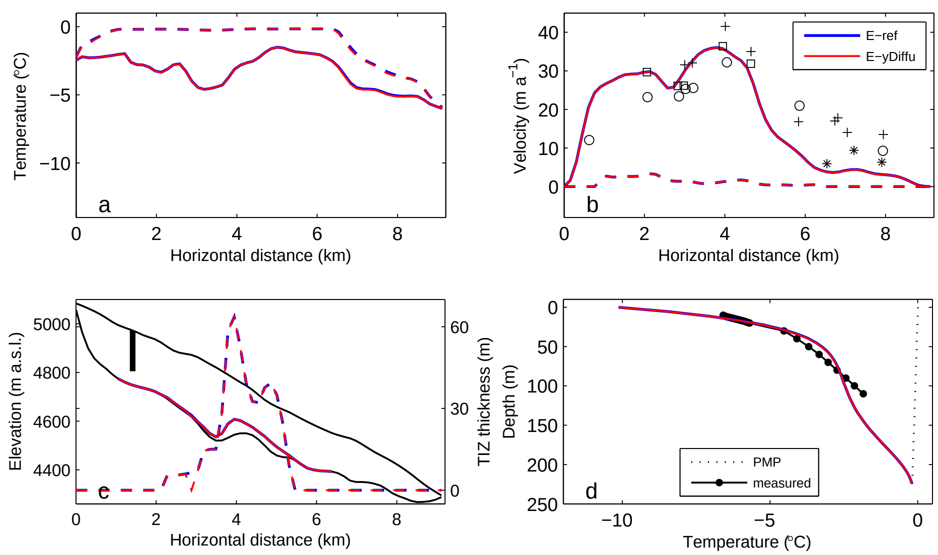

Figure 1: Modeled ice temperatures and velocities for experiments E-ref (blue line, without diffusion in y-axis) and E-yDiffu (red line, with parameterized diffusion in y-axis)

p5,26 What happens with water produced by dissipation? Does this stay in the ice, or does it drain at a certain volume ratio? Is a balance equation for the water content, or the enthalpy, solved?

We thank the reviewer for these very good questions! Sorry to admit that we've not considered those problems so far yet. We assume a constant water content in the temperate ice layer. But we haven't yet included a thermo-hydrological model. An enthalpy scheme for the polythermal glacier with a balance equation is under development.

p6,3 Even if the model is described elsewhere in detail, the main characteristics should be given here: solution method (finite difference, finite element, ...), discretization (element type, mesh size), solution method (solver, time-stepping, CFL condition) etc., and maybe some implementation details (solver libraries used, maybe Matlab, etc...).

The numerical implementations are the same as described in Zhang et al. (2013). We now have added a sub-section introducing the main features of the numerical solutions in p7–line19-25.

p6,7 Parentheses should be adapted using \left(and \right)

Corrected.

p6,11 Strictly, this should be $\sigma_n - P_w$ *using the normal stress on the bed, which might be quite different from the overburden calculated with the local vertical ice thickness. In which direction is* H *measured, vertically (along* z*), or perpendicular to the ice surface?*

Here H is vertical to the ice-bed interface (along z). The effective pressure used in the friction law is defined as the ice overburden pressure (see Gagliardini et al. (2007)), not the normal stress.

p6,30 This boundary condition is valid for cold ice, but what is used in temperate ice? There, any geothermal heat will contribute to melting.

If there is a temperate layer at the glacier base, two cases must be distinguished. For the melting case where cold ice flows into the temperate ice, we assume a negligible water content, and the ice temperature gradient at the CTS equals to the Clausius-Clapeyron gradient (β). For the freezing case where temperate ice flows into the cold ice, the latent heat released due to refreezing must be taken into account. We assume an ice temperature gradient at the CTS following Funk et al. (1994):

$$\frac{\partial T}{\partial z} = -\frac{Q_r}{k} + \beta. \tag{1}$$

The above description has been illustrated in the section 3.2.

p7,2 I assume that the G-term is not very important for the model results. In mountain topography, the geothermal heat flux can vary a lot on short spatial scales, so the importance of this should be at least discussed.

We now discuss the impacts of geothermal heat flux in our discussion section.

"Another uncertainty could be from the spatially uniform geothermal heat flux that we assume in the model, as it may have a great spatial variation due to the mountain topography (Lüthi and Funk, 2001)."

p7,22 So, the water content is assumed constant throughout the temperate ice? This *is problematic and will obviously introduce some inaccuracies.*

It's true that a constant water content may bring uncertainties in our results. Further efforts of including the water content computation and drainage system are still under development. We now have add a sentence for this in the discussion section.

"In addition, we can also improve our model ability by linking the water content in the temperate ice layer to a physical thermo-hydrological process in the future."

p8,3 "compare to"

Corrected.

p8,6 The omission of convergent flow is only one possible (and likely) explanation, but there might be others, e.g. basal motion. This statement should be made more carefully.

It's correct that our explanation is one of many possible reasons. The underestimation of the ice surface velocities may possibly result from the neglect of the convergent flow from the west branch and an enhanced basal sliding which is not captured by our model in the confluence area. To verify this hypothesis, we conduct two other experiments, E-W and E-WS. In E-W the glacier widths are increased by 450 m at km 5.8 – 7.3 as a proxy of including the impact of the convergent flow from the west branch (Fig. 2). In E-WS, except for the same glacier width increase as in E-W, we also increase $\lambda_{\max}$ by 200% and decrease $m_{\max}$ by 60% for accelerating the basal sliding at km 5.8 – 7.3 (Fig. 2). We can clearly find that while both factors have a non-negligible contribution to the model results, the basal sliding may play a bit more important role in the confluence area. This indicates a need of considering glacier flow branches and spatially variable sliding law parameters in real glacier modeling studies. See p9–line3-10.

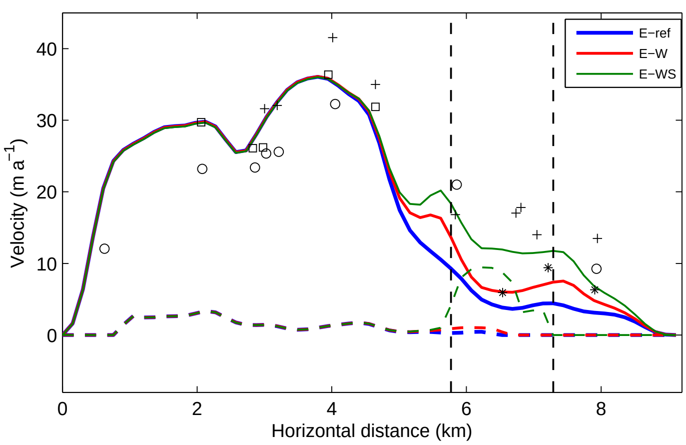

Figure 2: Modeled ice velocities for experiments E-ref (blue line), E-W (red line), and E-WS (green line). The glacier widths in the zone bounded by the vertical dashed lines are uniformly increased by 450 m.

p8,7 Here you should qualify "the modeled basal sliding velocities", IIUC. The reality, again, could be that basal sliding is much higher there. This could be elaborated upon in the Discussion.

Yes, we discuss the modeled basal sliding velocities here. As suggested by the reviewer, we have conducted two other experiments in which the glacier widths are increased and the sliding law parameters are spatially tuned in the confluence area (see the above response). Then we discussed the impacts of convergent effects of the west branch and basal sliding (see p9–line8-10).

p8,8 "observed": this is confusing, as you talk about model results. Better say: "the model predicts"

We now use "The model predicts a TIZ overlain by cold ice over a horizontal distance of km 1.1 – 6.5".

p8,9 add space between "110m"

Fixed.

p8,10 "ice fluxes" (not "ice flows")

Corrected.

p8,13 More important than matching temperatures would be a discussion of the heat fluxes. While the measurements show constant fluxes below 50 m depth below the surface, the model shows zones of warming and cooling (bends in the temperature profile). It would be important to understand the reason for these excursions from a straight line, is the shape of this profile due to advection, dissipation, or due the temperature history?
Closer to the surface (above 50 m depth) the measured gradient is much higher, which might reflect the thermal properties of the firn in a steady state (lower conductivity k). Since ice conductivity is assumed everywhere in the model, this might explain the difference there (cf. Fig. 5 in Luthi and Funk (2001) for a theoretical temperature profile with firn).

This is a good question. To account for the thermal properties of the firn as suggested by the reviewer, we lower the conductity ($k = 0.17$ W m^{-1} K^{-1}) of the surface layer in the accumulation zone (experiment E-FC). Compared with the reference experiment (E-ref), E-FC results in higher temperature gradient above 60 m depth (Fig. 3a). Nevertheless, this cannot explain the deviation of the modeled temperature profile from a nearly straight line below 30 m depth. We also conduct other experiments to investigate the possible factors affecting the shape of the modeled temperature profile by adjusting the parameters, i.e., ELA, firn temperature and horizontal grid resolution. We find that the bend of the modeled temperature profile at the borehole is strongly influenced by the discontinuous thermal surface boundary condition accross the accumulation and ablation zones. The borehole is located in the upper ablation area (4971 m a.s.l.), and is close to the snow line (around 4980 m a.s.l.). Therefore, the modeled temperature at the borehole can be influenced by the horizontal advection of relatively warm ice due to released latent heat from the accumulation zone. The higher temperature gradient in the upper part of the modeled profile demonstrates the impacts of horizontal heat advection from the upstream. We also compare the modeled temperature profiles below the borehole, which show little impacts from the upstream heat advection (Figure 3b).

In 2011, we observed that the ice drilled below the depth of 166 m was wet, indi-

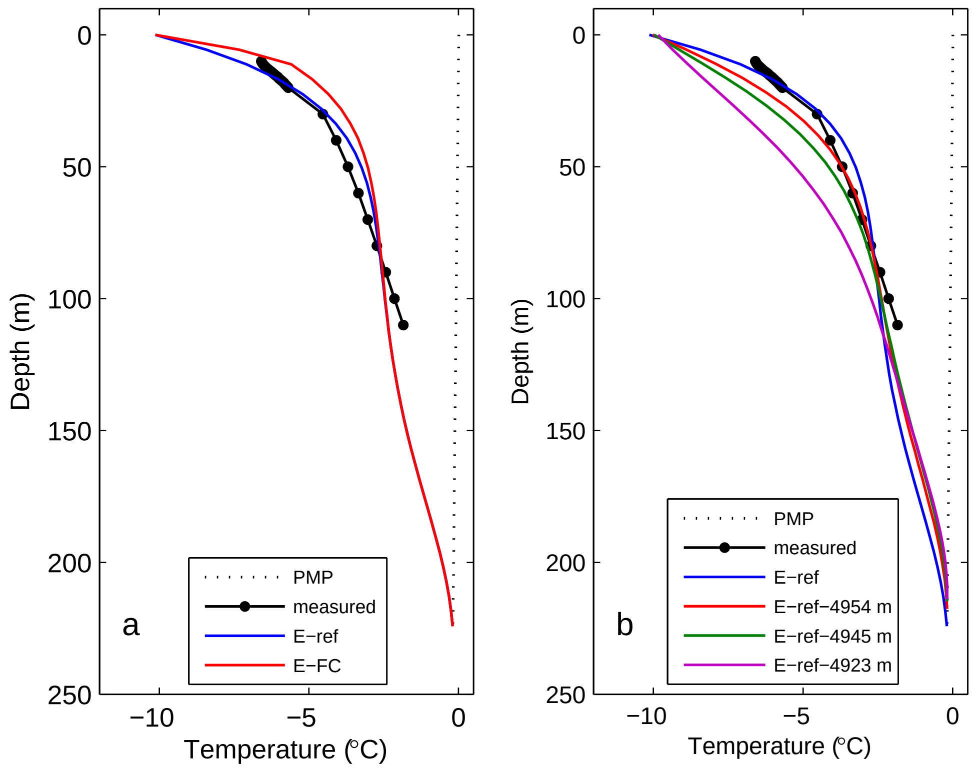

Figure 3: (a) Comparison of modeled temperature profiles at the borehole site. Blue line shows the modeled temperature in the reference experiment, while red line shows the result of experiment E-FC in which the firn conductivity is taken into account. (b) Comparison of modeled temperature profiles in the reference experiment. Blue line shows the modeled temperature at the deep borehole (4971 m a.s.l.). The red, green and purple lines show the modeled temperature profiles at 4954 m a.s.l., 4945 m a.s.l. and 4923 m a.s.l., respectively. Measured borehole temperatures are shown in dots. The pressure-melting point is shown by the dotted line.

cating the temperate ice layer there was possibly thicker than our model prediction (around 5.6 m). As our 2D flow-band model assumes a simple parameterization of the surface thermal boundary conditions, and neglects the convergent flow from the other cirques, it cannot capture the complex heat flow at the deep borehole site. In the future, we may perhaps try a 3D Stokes model and see if there would be something different.

p8,27 It would be helpful to also show a graph of TIZ thickness (a second panel in Fig. 8c). It appears that the bed is temperate almost everywhere in the blue and *green model runs, but with very small TIZ.*

Good suggestions. We have shown the TIZ thicknesses in the double-Y-axis graphs, i.e. Fig. 10c, 11c and 12c. It's correct that a large region of the bed is temperate as predicted by the experiments E-ref and E-20m. Thick temperate basal ice appears in km 2 – 6, while temperate ice in other places is only one layer.

p8,31 "above" (leave away "in")

We now delete "in".

p9,11 ff instead of "drop" and "remove" you could consistently use "neglect" or "leave away"

Thanks. We now use "neglect" and "leave away".

p9,25 qualify basal sliding by modeled

Corrected.

p9,28 leave away "higher-order"

Changed.

p10,2 "physically" should be "physical"

Corrected.

p10,9 consolidate the two citations

Corrected.

p10,11 Past changes can have a very important impact (see for example Luthi et al. (2015)), as are warming processes in the firn (e.g. Machguth et al. (2016))

The corresponding sentences have been reformulated as "The assumption of steady state neglects the transient effects of past climate and glacier changes, which can have a very important impact on the shape of temperature profile (Lüthi et al., 2015; Gilbert et al., 2015).".

p11,16 Replace "e.g." with "of" (these are not just examples, but an exhaustive list of measurements used in the study).

Fixed.

p11,21 No need to show the symbol "(u)" here again (leave away).

We now delete "(u)".

Fig 1 A nice overview photograph would help setting the scene for this remote glacier that most readers wont know.

Good suggestion. We now use a Landsat 8 satellite image of LHG12 Glacier.

Fig 2 same labels on the horizontal axis of Figs. 3 and 4 would ease of comparison.

Fixed.

Fig 8d Caption: modeled and measured (lines vs symbols) should be interchanged.

Corrected.

References

Funk, M., Echelmeyer, K. A., and Iken, A.: Mechanisms of fast flow in Jakobshavn Isbræ, West Greenland: Part II. Modeling of englacial temperatures, Journal of Glaciology, 40, 569–585, 1994.

Gagliardini, O., Cohen, D., Råback, P., and Zwinger, T.: Finite-element modeling of subglacial cavities and related friction law, Journal of Geophysical Research, 112, F02 027, 2007.

Pattyn, F.: Transient glacier response with a higher-order numerical ice-flow model, Journal of Glaciology, 48, 467–477, 2002.

Zhang, T., Xiao, C., Colgan, W., Qin, X., Du, W., Sun, W., Liu, Y., and Ding, M.: Observed and modelled ice temperature and velocity along the main flowline of East Rongbuk Glacier, Qomolangma (Mount Everest), Himalaya, Journal of Glaciology, 59, 438–448, 2013.

Response to K. Poinar

Yuzhe Wang

We would like to thank Dr. K. Poinar for giving constructive and encouraging comments on our paper; they were very helpful to improve our manuscript. Our responses to all the comments are given below. The original reviewer's comments are given in italic, and our responses are given directly below in regular.

Specific comments

*The model appears to be state-of-the-art, and the limits of its application are discussed (omission of west branch). I think it would be beneficial to include a bit more discussion (and perhaps, but not necessarily, numeric estimation) of how inclusion of the secondary branch of the glacier would improve the results. (I think *why* it should improve the results is clear, but *how much* is not clear, and *where* is not in the expected locations.) To be clearer on my *where* point: it appears that the area of largest disagreement between measured/modeled velocities (5.3 to 7 km) occurs just upstream of the junction with the west branch (4500m elevation or 7 km). One would expect any effects of the west branch to be downstream of the junction.*

Thanks for your good suggestion. The underestimation may possibly result from

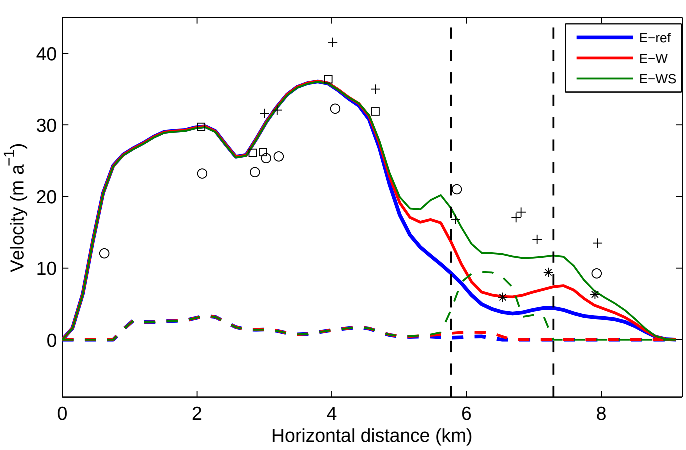

Figure 1: Modeled ice velocities for experiments E-ref (blue line), E-W (red line), and E-WS (green line). The glacier widths in the zone bounded by the vertical dashed lines are uniformly increased by 450 m.

the neglect of the convergent flow from the west branch and an enhanced basal sliding which is not captured by our model in the confluence area (see our responses to the other two reviewers). To verify this hypothesis, we conduct two other experiments, E-W and E-WS. In E-W the glacier widths are increased by 450 m at km 5.8 – 7.3 as a proxy of including the impact of the convergent flow from the west branch (Fig. 1). In E-WS, except for the same glacier width increase as in E-W, we also increase $\lambda_{\max}$ by 200% and decrease $m_{\max}$ by 60% for accelerating the basal sliding at km 5.8 – 7.3 (Fig. 1). We can clearly find that while both factors have a non-negligible contribution to the model results, the basal sliding may play a bit more important role in the confluence area. The basal sliding velocities in experiment E-WS can be raised to 9.5 m a^{-1} at km 6.2. The mean ice surface velocities modeled by E-W and E-WS in the distance of km 5.3 – 9.1, are larger than those of E-ref by 2.1 m a^{-1} and 4.9 m a^{-1}, respectively. This indicates a need of considering glacier flow branches and spatially variable sliding law parameters in real glacier modeling studies.

This paper also appears to be the first presentation of the temperature data from the four boreholes, so a little more detail here would be appropriate. The description of the three shallow boreholes is more complete than for the deeper, and I would argue more important to the paper, borehole. For instance, how long were the sensors operational within the ice (were the temperatures able to equilibrate), and what is the error on the readings? How precise are the depths? The data in Figure 4(b) look smoother than I have usually seen from deep boreholes, leading to these questions.

Good suggestions. We now have added more details about the measurement of deep borehole temperatures.

"To determine the englacial thermal conditions of LHG12, we drilled a deep ice core (167 m) in the upper ablation area of LHG12 (approximately 4971 m a.s.l., Fig. 1). In October 2011, ice temperature were measured to a depth of approximately 110 m using a thermistor string after 20 days of the drilling, as shown in Fig. 4d. The string consists of 50 temperature sensors with a vertical spacing of 0.5 m and 10 m at the ice depths of 0 – 20 m and 20 – 110 m, respectively. The accuracy of the temperature sensor is around $\pm 0.05\,^{\circ}$C (Liu et al., 2009)."

My other suggestion is to improve the clarity of Figures 5, 6, and 7. Although the legends do indicate what is being plotted, they are small and encoded. This could be fixed easily by adding a title to each plot ("Varying bedrock bump wavelength") and/or adding this to the caption.

This is a good idea, and we now have added the title for each panel.

The caption for Figure 9(d) gets measured / modeled temperatures backwards.

Fixed.

An investigation of the thermo-mechanical features of Laohugou Glacier No.12 in Mt. Qilian Shan, western China, using a two-dimensional first-order flow-band ice flow model

Yuzhe Wang[1,2], Tong Zhang[3,1], Jiawen Ren[1], Xiang Qin[1], Yushuo Liu[1], Weijun Sun[4], Jizu Chen[1,2], Minghu Ding[3], Wentao Du[1,2], and Dahe Qin[1]

[1]State Key Laboratory of Cryospheric Sciences, Cold and Arid Regions Environmental and Engineering Research Institute, Chinese Academy of Sciences, Lanzhou 730000, China
[2]University of Chinese Academy of Sciences, Beijing 100049, China
[3]Insititute of Climate System & Polar Meteorology, Chinese Academy of Meteorological Sciences, Beijing 100081, China
[4]College of Geography and Environment, Shandong Normal University, Jinan 250014, China

Correspondence to: Tong Zhang (tzhang@camscma.cn)

Abstract. ~~En-glacial thermal conditions are very important for controlling ice rheology.~~ By combining *in situ* measurements and a two-dimensional thermo-mechanically coupled ice flow model, we investigate the present thermal status of the largest valley glacier (Laohugou Glacier No.12; LHG12) in Mt. Qilian Shan located in the arid region of western China. Our model results suggest that LHG12, previously considered as fully cold, is probably polythermal, with a lower temperate ice layer ~~(approximately 5.4 km long)~~ overlain by an upper layer of cold ice over a large region of the ablation area. ~~Generally, modelled~~ Modeled ice surface velocities match well with the *in situ* observations in the east branch (mainstream) ~~well~~ but clearly underestimate the ice surface velocities near the glacier terminus possibly because the convergent flow ~~of the west branch is ignored. The modelled~~ is ignored and the basal sliding beneath the confluence area is underestimated. The modeled ice temperatures agree ~~closely~~ with the *in situ* measurements (with biases less than 0.5 K) from a deep borehole (110 m) in the upper ablation area. The model results ~~were~~ are highly sensitive to surface thermal boundary conditions, for example, surface air temperature and near-surface ice temperature. In this study, we ~~suggest using a combination of surface air temperatures and near-surface ice temperatures(following the work of Wohlleben et al. , 2009) as Dirichlet surface thermal conditions to include the contributions of the latent heat released during refreezing of surface melt-water in the accumulation zone.~~ use a Dirichlet surface thermal condition constrained by 20 m borehole temperatures and annual surface air temperatures. Like many other alpine glaciers, strain heating is ~~the most~~ an important parameter controlling the ~~en-glacial~~ englacial thermal structure in LHG12.

1 Introduction

The storage of water in glaciers is an important component of the hydrological cycle at different time scales (Jansson et al., 2003; Huss et al., 2010), especially in arid and semi-arid regions such as northwestern China, where many glaciers are currently retreating and disappearing (Yao et al., 2012; Neckel et al., 2014; Tian et al., 2014). ~~As a very important water source for the inhabitants of northwestern China, Mt. Qilian Shan (MQS), which is located~~ Located on the northeastern edge of the Tibetan

Plateau (36 – 39 °N, 94 – 104 °E), ~~develops approximately~~ Mt. Qilian Shan (MQS) develops 2051 glaciers ~~that cover~~ covering an area of approximately 1057 km^2 ~~and have~~ with a total ice volume of approximately 50.5 km^3 (Guo et al., 2014, 2015). Meltwater from MQS glaciers is a very important water resource for the agricultural irrigation and socio-economic development of the oasis cities in northwestern China. Thus, the changes in the MQS glaciers that occur as the climate becomes warmer in the near future are of concern.

Due to logistic difficulties, few MQS glaciers have been investigated in previous decades. However, Laohugou Glacier No.12 (hereafter referred to as LHG12), the largest valley glacier of MQS, has been investigated. Comprised of two branches (east and west), LHG12 is located on the north slope of western MQS (39°27' N, 96°32' E; Fig. 1), with a length of approximately 9.8 km, an area of approximately 20.4 km^2, and an elevation range of 4260 – 5481 m a.s.l. (Liu et al., 2011). LHG12 was first studied by a Chinese expedition from 1958 – 1962 and was considered again in short-term field campaigns in the 1970s and 1980s that were aimed at monitoring glacier changes (Du et al., 2008). Since 2008, the Chinese Academy of Sciences has operated a field station for obtaining meteorological and glaciological measurements of LHG12.

The temperature distribution of a glacier primarily controls the ice ~~flow rheology, en-glacial~~ rheology, englacial hydrology, and basal sliding conditions ~~of the glacier~~ (Blatter and Hutter, 1991; Irvine-Fynn et al., 2011; Schäfer et al., 2014). ~~For example, the existence of basal temperate ice was responsible for modelled velocity biases in a first-order model when compared with the "full" Stokes modelling approach . In addition,~~ A good understanding of the glacier thermal conditions is importance for predicting glacier response to climate change (Wilson et al., 2013; Gilbert et al., 2015), improving glacier hazard analysis (Gilbert et al., 2014a), and reconstructing past climate histories (Vincent et al., 2007; Gilbert et al., 2010). The thermal regime of a glacier ~~can be strongly influenced~~ is mainly controlled by the surface thermal boundary conditions (e.g., Gilbert et al., 2014b; Meierbachtol et al., 2015). For example, near-surface warming from refreezing ~~melt-water~~ meltwater and cooling from the cold air of crevasses influence the thermal regimes of glaciers (Wilson and Flowers, 2013; Wilson et al., 2013; Gilbert et al., 2014a). Using both *in situ* measurements and numerical models, Meierbachtol et al. (2015) argued that shallow borehole ice temperatures served as better boundary constraints than surface air temperatures in Greenland. However, for the east Rongbuk glacier on Mt. Everest, which is considered polythermal, Zhang et al. (2013) found that the ~~modelled~~ modeled ice temperatures agreed well with the *in situ* shallow borehole observations when using surface air temperatures as the surface thermal boundary condition. Therefore, careful investigation of the upper thermal boundary condition is highly necessary for glaciers in different regions under different climate conditions.

LHG12 is widely considered as an extremely ~~continental-type~~ continental type (cold) glacier and is characterized by low temperatures and precipitation (Huang, 1990; Shi and Liu, 2000). However, in recent years, we have observed extensive and widespread ~~melt-water~~ meltwater at the ice surfaces and glacier terminus. In addition, percolation of snow ~~melt-water~~ meltwater consistently occurs in the accumulation basin during the summer. Therefore, we address the following two pressing questions in this study: (i) What is the present thermal status of LHG12? and (ii) How do different surface thermal boundary conditions impact the ~~modelled~~ modeled ice temperature and flow fields? Because warm ice can assist basal slip and accelerate glacier retreat, understanding the current thermal status of LHG12 is very important for predicting its future dynamic behaviour.

To answer these questions, we conduct diagnostic simulations for LHG12 by using a thermo-mechanically coupled first-order flow-band ice flow model. This paper is organized as follows: First, we provide a detailed description of the glaciological ~~dataset~~ datasets of LHG12. Then, we briefly review the numerical ice flow model used in this study. After performing a set of model sensitivity experiments, we compare the model results with the measured ice surface velocities and the ice temperature profile obtained from a deep borehole. Next, we investigate the impacts of different ~~thermal surface~~ surface thermal boundary conditions and assess the contributions of heat advection, strain heating, and basal sliding to the temperature field of LHG12. Finally, we discuss the limitations of our model and present the important conclusions that resulted from this study.

2 Field data

Most *in situ* observations, e.g., borehole ice temperatures, surface air temperatures and ice surface velocities, have been made on the east branch (mainstream) of LHG12 (Fig. 1). Measurements on the west branch are dispersed and temporally discontinuous. Thus, we only consider the *in situ* data from the east tributary when building our numerical ice flow model.

2.1 Glacier geometry

In July – August 2009 and 2014, two ground-penetrating radar (GPR) surveys were conducted on LHG12 using a pulseEKKO PRO system with center frequencies of 100 MHz (2009) and 50 MHz (2014) (Fig. 1~~).~~ b). Wang et al. (2016) have presented details regarding the GPR data collection and post-processing.

As shown in Fig. 2a, the east branch of LHG12 has a mean ice thickness of approximately 190 m. We observed the thickest ice layer (approximately 261 m) at 4864 m a.s.l. Generally, the ice surface of LHG12 is gently undulating, with a mean slope of 0.08°, and the bed of LHG12 shows significant ~~over-deepening~~ overdeepening in the middle of the center ~~flow-line~~ flowline (CL) (Fig. 2a). ~~The transverse profiles of the glacier can be described by the~~ To account for the lateral effects exerted by glacier valley walls in our 2D ice flow model, we parameterize the lateral drag using the glacier half widths. Based on the GPR measurements on LHG12, we parameterize the glacier cross-sections by a power law function ~~$d = aL^b$, where d and L~~ $z = aW(z)^b$, where z and $W(z)$ are the vertical and horizontal distances from the lowest point of the profile, and a and b are constants ~~that represent~~ representing the flatness and steepness of the glacier valley, respectively (Svensson, 1959). The b values for LHG12 range from 0.8 to 1.6, indicating that the valley containing LHG12 is approximately "V"-shaped (Wang et al., 2016). As an input for the flow-band ice flow model, the glacier width, W, was also calculated by ignoring all tributaries (including the west branch) (Fig. 1b and 2b).

2.2 Ice surface velocities

The surface velocities of the ice in LHG12 were determined from repeated surveys of stakes drilled into the ice surface. All stakes were located in ~~an elevation span~~ the distance between km 0.6 – 7.9 along the CL (Fig. 3), spanning an elevation range of 4355 – 4990 m.a.s.l. (Fig. 1b). We measured the stake positions using a real-time kinematic (RTK) ~~method~~ fixed solution by a South Lingrui S82 GPS system (Liu et al., 2011). The accuracy of the GPS positioning is an order of a few centimeters and the uncertainty of the calculated ice surface velocties is estimated to be less than 1 m a^{-1}. Because it is difficult to conduct fieldwork on LHG12 (due to, e.g., crevasses and supra-glacial streams), it was nearly impossible to measure all stakes each observational year. Thus, the current dataset includes annual ice surface velocities from 2008 – 2009 and 2009 – 2010, summer measurements from June 17 – August 30, 2008, and winter measurements from February 1 – May 28, 2010.

The *in situ* ice surface velocities shown in Fig. 3 are all from stakes near the CL (Fig. 1b). Small ice surface velocities ($<$ 17 m a^{-1}) are clearly visible in the upper accumulation (km 0 – 1.2) and lower ablation areas (km 6.5 – 9.0) (Fig. 3). Fast ice flow ($>$ 30 m a^{-1}) can be observed between elevations of 4700 – 4775 m a.s.l. (km 4.0 – 5.0), where the ice surface velocities during the summer are approximately 6 m a^{-1} greater than the annual mean velocity ($<$ 40 m a^{-1}). Measurements of winter ice surface velocities ($<$ 10 m a^{-1}) are only available near the glacier terminus showing a clear inter-annual variation of ~~ice speed~~the ice flow speeds.

2.3 Surface air temperature

Two automatic weather stations (AWS) were deployed on LHG12, one in the ablation area at 4550 m a.s.l. (site 1, ~~see~~ Fig. 1b), and one in the accumulation area at 5040 m a.s.l. (site 3). During the period of 2010 – 2013, the mean annual air temperatures (2 m above the ice surface) at sites 1 and 3 were $-9.2\,^{\circ}$C and $-12.2\,^{\circ}$C, respectively, suggesting a lapse rate of -0.0061 K m^{-1}. These results were used to calculate the distribution of the surface air temperatures at all elevations on LHG12.

2.4 Borehole ice temperature

In August 2009 and 2010, we drilled three ~~25m~~ 25 m deep shallow boreholes on LHG12 (Fig. 1b). One borehole was drilled in the upper ablation area (site 2, approximately 4900 m a.s.l.) and two boreholes were drilled at the AWS locations (sites 1 and 3). The snow/ice temperatures were measured at the boreholes during the period of October 1, 2010 – September 30, 2011. The seasonal variations of the snow/ice temperatures in the shallow boreholes are presented in Figs. 4a, b and c. Our measurements show very little fluctuation ($\pm$0.4 K) in the ice temperatures over the depth range of 20 – 25 m. Below the 3 m depth, the annual mean temperature profiles for sites 1 and 2 show a linearly increase in temperature with depth, while the annual mean temperature profile for site 3 is convex upward. The mean annual ~~ice temperatures at a depth of~~ 20 m ice temperatures ($T_{20\mathrm{m}}$) at sites 1, 2, and 3 are 5.5 K, 3.0 K, and 9.5 K higher than the mean annual air temperatures (T_{air}), respectively. Despite its higher elevation, the near-surface snow/ice temperatures below a depth of 5 m at site 3 are greater than the near-surface snow/ice temperatures in the ablation area (sites 1 and 2), largely due to the latent heat released as the ~~melt-water~~ meltwater entrapped in the surface snow layers refreezes, as observed in many previous field expeditions.

To determine the ~~en-glacial~~ englacial thermal conditions of LHG12, we drilled a deep ice core (167 m) in the ~~lower accumulation~~ upper ablation area of LHG12 (approximately 4971 m a.s.l., Fig. 1~~). Ice temperature data were obtained~~ b). In October 2011, ice temperature were measured to a depth of approximately 110 m using a thermistor string after 20 days of the drilling, as shown in Fig. 4d. ~~We can clearly see that the ice temperature largely increases from -10°C at the surface to -6°C at the depth of 4 m . At the depth of 9 m , the ice temperature lowers to a minimum value of -6.6°C. In the range of 9 m~~ The string consists of 50 temperature sensors with a vertical spacing of 0.5 m and 10 m at the ice depths of 0 – ~~30 mdepth, the~~

~~temperature~~ 20 m and 20 – 110 m, respectively. The accuracy of the temperature sensor is around ± 0.05 K (Liu et al., 2009). From Fig. 4d we can see that the temperature profile is close to linear with a temperature gradient of ~~about +~~around 0.1 K m^{-1} at the depths of 9 – 30 m. Below the depth of 30 m, the ice temperature also demonstrates a linear relationship with depth but with a smaller temperature gradient of ~~about +~~around 0.034 K m^{-1}.

3 Model description

In this study, we used the same two-dimensional (2D), thermo-mechanically coupled, first-order, flow-band ice flow model as Zhang et al. (2013). Therefore, we only address a very brief review of the model here.

3.1 Ice flow model

We define x, y, and z as the horizontal along-flow, horizontal across-flow and vertical coordinates, respectively. ~~The glacier force balance equation~~ By assuming the vertical normal stress as hydrostatic and neglecting the bridging effects (Pattyn, 2002), the equation for momentum balance is given as ~~follows:~~

$$\frac{\partial}{\partial x}(2\sigma'_{xx}+\sigma'_{yy})+\frac{\partial \sigma'_{xy}}{\partial y}+\frac{\partial \sigma'_{xz}}{\partial z}=\rho g\frac{\partial s}{\partial x}, \tag{1}$$

where σ'_{ij} is the deviatoric stress tensor, ρ is the ice density, g is the gravitational acceleration, and s is the ice surface elevation. The parameters used in this study are given in Table 1.

The constitutive relationship of ice dynamics is described by the Glen's flow law ~~as follows~~ (Cuffey and Paterson, 2010) ~~:~~

$$\sigma'_{ij}=2\eta\dot{\epsilon}_{ij},\quad \eta=\frac{1}{2}A^{-1/n}(\dot{\epsilon_e}+\dot{\epsilon}_0)^{(1-n)/n}, \tag{2}$$

where η is the ice viscosity, $\dot{\epsilon}_{ij}$ is the strain rate, n is the flow law exponent, A is the flow rate factor, $\dot{\epsilon_e}$ is the effective strain rate, and $\dot{\epsilon}_0$ is a small number used to avoid singularity. The flow rate factor is parameterized using the Arrhenius relationship as ~~follows:~~

$$A(T)=A_0\exp(-\frac{Q}{RT}), \tag{3}$$

where A_0 is the pre-exponential constant, Q is the activation energy for creep, R is the universal gas constant, and T is the ice temperature. The effective strain rate $\dot{\epsilon_e}$ is related to the velocity gradient ~~as follows:~~ by

$$\dot{\epsilon}_e^2\simeq\left(\frac{\partial u}{\partial x}\right)^2+\left(\frac{\partial v}{\partial y}\right)^2+\frac{\partial u}{\partial x}\frac{\partial v}{\partial y}+\frac{1}{4}\left(\frac{\partial u}{\partial y}\right)^2+\frac{1}{4}\left(\frac{\partial u}{\partial z}\right)^2, \tag{4}$$

where u and v are the velocity components along the x and y direction, respectively. By assuming $\partial v/\partial y=(u/W)(\partial W/\partial x)$, we parameterize the lateral drag, ~~σ_{xy}~~ σ'_{xy}, as a function of the flow-band half width, W, ~~as follows :~~ following Flowers et al. (2011)

$$\sigma'_{xy}=-\frac{\eta u}{W}. \tag{5}$$

For an easy numerical implementation, we reformulate the momentum balance equation (1) as

$$\frac{u}{W}\left\{2\frac{\partial \eta}{\partial x}\frac{\partial W}{\partial x}+2\eta\left[\frac{\partial^2 W}{\partial x^2}-\frac{1}{W}\left(\frac{\partial W}{\partial x}\right)^2\right]-\frac{\eta}{W}\right\}$$
$$+\frac{\partial u}{\partial x}\left(4\frac{\partial \eta}{\partial x}+\frac{2\eta}{W}\frac{\partial W}{\partial x}\right)+\frac{\partial u}{\partial z}\frac{\partial \eta}{\partial z}+4\eta\frac{\partial^2 u}{\partial x^2}+\eta\frac{\partial^2 u}{\partial z^2}=\rho g\frac{\partial s}{\partial x}, \tag{6}$$

where the ice viscosity is defined as

$$\eta=\frac{1}{2}A^{-1/n}\left[\left(\frac{\partial u}{\partial x}\right)^2+\left(\frac{u}{W}\frac{\partial W}{\partial x}\right)^2+\frac{u}{W}\frac{\partial u}{\partial x}\frac{\partial W}{\partial x}+\frac{1}{4}\left(\frac{\partial u}{\partial z}\right)^2+\frac{1}{4}\left(\frac{u}{W}\right)^2+\dot{\epsilon}_0^2\right]^{(1-n)/2n}. \tag{7}$$

3.2 Ice temperature model

~~The~~ The ice temperature field can be calculated using a 2D ~~temperature model, where the horizontal diffusion is parameterized by glacier width, is given by~~ heat transfer equation (Pattyn, 2002),

$$k\left(\frac{\partial^2 T}{\partial x^2}+\frac{1}{W}\frac{\partial W}{\partial x}\frac{\partial T}{\partial x}+\frac{\partial^2 T}{\partial z^2}\right)-\rho c_p\left(u\frac{\partial T}{\partial x}+w\frac{\partial T}{\partial z}\right)+4\eta\dot{\epsilon}_e{}^2=0, \tag{8}$$

where w is the vertical ice velocity, k and c_p are the thermal conductivity and heat capacity of the ice, respectively.

The pressure melting point of the ice, T_{pmp}, is described by the Clausius-Clapeyron relationship ~~as follows:~~

$$T_{\text{pmp}}=T_0-\beta(s-z), \tag{9}$$

where T_0 is the triple-point temperature of water and β is the Clausius-Clapeyron constant. Following Zhang et al. (2013), we determined the position of the cold-temperate ice transition surface (CTS) by considering the following two cases: (i) melting condition, i.e., cold ice flows downward into the temperate ice zone, and (ii) freezing condition, i.e., temperate ice flows upward into the cold ice zone (Blatter and Hutter, 1991; Blatter and Greve, 2015). For the melting case, the ice temperature profile at the CTS simply follows a Clausius-Clapeyron gradient (β). However, for the freezing case, the latent heat, Q_r, that is released when the water contained in the temperate refreezes is determined as ~~follows~~ (Funk et al., 1994) ~~:~~

$$Q_r=w\omega\rho_w L, \tag{10}$$

where ω is the fractional water content of the temperate ice, ρ_w is the water density and L is the latent heat of freezing. In this case, following (Funk et al., 1994), the ice temperature gradient at the CTS can be described as ~~follows :~~

$$\frac{\partial T}{\partial z}=-\frac{Q_r}{k}+\beta. \tag{11}$$

3.3 Boundary conditions

In the ice flow model, we assume a stress-free condition for the glacier surface, and use the Coulomb friction law to describe the ice-bedrock interface where the ice slips (Schoof, 2005)~~.~~,

$$\tau_b=\Gamma\left(\frac{u_b}{u_b+\Gamma^n N^n\Lambda}\right)\left(\frac{u_b}{u_b+\Gamma^n N^n\Lambda}\right)^{1/n}N, \qquad \Lambda=\frac{\lambda_{\text{max}}A}{m_{\text{max}}}, \tag{12}$$

where τ_b and u_b are the basal drag and velocity, respectively, N is the basal effective pressure, λ_{max} is the dominant wavelength of the bed bumps, m_{max} is the maximum slope of the bed bumps, and Γ and Λ are geometrical parameters (Gagliardini et al., 2007). Here we take $\Gamma = 0.84 m_{\text{max}}$ following Flowers et al. (2011) and Zhang et al. (2013). The basal effective pressure in the friction law, N, is defined as ~~follows:~~ the difference between the ice overburden pressure and the basal water pressure (Gagliardini et al., 2007; Flowers et al., 2011),

$$N = \rho g H - P_w = \phi \rho g H, \tag{13}$$

where H and P_w are the ice thickness and basal water pressure, respectively, and ϕ implies the ratio of basal effective pressure to the ice overburden pressure. The basal drag is defined as the sum of all resistive forces (Van der Veen, 1989; Pattyn, 2002). It should be noted that the basal sliding is only permitted when basal ice temperature reaches the local pressure-melting point.

We apply a Dirichlet temperature constraint (T_{sbc}) on the ice surface in the temperature model. In some studies, $T_{\text{sbc}} = T_{\text{air}}$ is used (e.g. Zhang et al., 2013), which, as suggested by recent studies, could result in lower velocity values (Sugiyama et al., 2014) and cold bias in ice temperature simulations (Meierbachtol et al., 2015). By contrast, Meierbachtol et al. (2015) recommended using the snow/ice temperature at the depth where inter-annual variations of air temperatures are damped (15 – 20 m, T_{dep}) (a proxy for the annual mean ice surface temperature). One advantage of using T_{dep} is that the effects of refreezing ~~melt-water~~ meltwater and the thermal insulation of winter snow can be included in the model (Huang et al., 1982; Cuffey and Paterson, 2010). In fact, the condition $T_{\text{dep}} = T_{\text{air}}$ is acceptable only in dry and cold snow zones (Cuffey and Paterson, 2010); however, $T_{\text{dep}} > T_{\text{air}}$ is often observed in zones where ~~melt-water~~ meltwater is refreezing in glaciers, such as the LHG12 ~~glacier~~ (Fig. 4). ~~When including the impacts of ice advection, suggested using a mean value of T_{dep} and T_{air} for the ablation surface.~~ In this study, we ~~adopt the method presented by by setting~~ set T_{sbc} in the accumulation zone to the 20 m borehole temperature measured at site 3, while T_{sbc} in the ablation area is prescribed by a simple parameterization (Lüthi and Funk, 2001; Gilbert et al., 2010)

$$T_{\text{sbc}} = \begin{cases} T_{20\text{m}}, & \text{in the accumulation zone,} \\ \cancel{T_{20\text{m}}}T_{\text{air}} + \cancel{T_{\text{air}}/2}c, & \text{in the ablation zone,} \end{cases} \tag{14}$$

~~which is denoted as a~~ where c is a tuning parameter including the impacts of both the surface energy budget and the steady-state temperature (Gilbert et al., 2010). We denote Eq. (14) as the surface thermal boundary condition of the reference experiment (E-ref) after comparing the other two numerical experiments by setting $T_{\text{sbc}} = T_{\text{air}}$ (E-air) and $T_{\text{sbc}} = T_{20\text{m}}$ (E-20m) (see Sect. 4.3 for details). ~~The T_{sbc} values in the ablation area are parameterized as a linear function of elevation and the environmental lapse rate using the measurements from sites 1 and 2, and all T_{sbc} values in the accumulation basin are set to $T_{20\text{m}}$ for site 3.~~

At the ice-bedrock interface, we apply the following Neumann-type boundary condition in the temperature model~~:~~,

$$\frac{\partial T}{\partial z} = -\frac{G}{k}, \tag{15}$$

where G is the geothermal heat flux. We here use a constant geothermal heat flux, 40 mW m^{-2}, an *in situ* measurement from the Dunde ice cap in the western MQS (Huang, 1999), over the entire model domain.

3.4 Numerical solution

In our model we use a finite difference discretization method and a terrain-following coordinate transformation. The numerical mesh we use contains 61 grids in x and 41 layers in z. The ice flow model (Eq. (6)) is discretized with a second-order centered difference scheme while the ice temperature model (Eq. (8)) employs a first-order upstream difference scheme for the horizontal heat advection term and a node-centered difference scheme for the vertical heat advection term and the heat diffusion terms. The velocity and temperature fields are iteratively solved by a relaxed Picard subspace iteration scheme (De Smedt et al., 2010) in Matlab.

4 Model results and discussions

To understand the present thermal status of LHG12, we assume a thermal steady-state condition and perform a series of thermo-mechanically coupled diagnostic simulations using a 2D first-order flow-band model (described in above). First, we simulate the ice velocity and temperature fields for LHG12 by investigating the sensitivities of the model to geometrical bed parameters ($\lambda_{\max}$ and $m_{\max}$), ratio of basal effective pressure (ϕ), water content (ω), geothermal heat flux (G)~~and the~~ , valley shape index (b)~~. Then, we~~ , and surface thermal boundary parameter c. We then inspect three different surface thermal boundary conditions (E-ref, E-air, and E-20m) by comparing their model outputs with *in situ* ice temperature observations in the deep borehole at site 3. In addition, we perform four experiments (E-advZ, E-advX, E-strain, and E-slip) to investigate the impacts of heat advection, strain heating, and basal sliding on the thermal field and flow characteristics of LHG12.

4.1 Parameter sensitivity

As shown in Figs. 5 and 6, we conduct a series of sensitivity experiments to investigate the relative importance of different model parameters ($\lambda_{\max}$, $m_{\max}$, ϕ, ω, G, b, c) on ice flow speeds and temperate ice zone (TIZ) sizes by varying the value of one parameter while holding the other parameters fixed.

The friction law parameters, $\lambda_{\max}$ and $m_{\max}$, which describe the geometries of bedrock obstacles (Gagliardini et al., 2007; Flowers et al., 2011), have non-negligible impacts on the model results. As shown in Figs. 5a and b, the ~~modelled~~ modeled velocities and TIZ sizes increase as $\lambda_{\max}$ increases and $m_{\max}$ decreases, similar to in the results observed by Flowers et al. (2011) and Zhang et al. (2013). A large increase in the ~~modelled~~ modeled velocity occurs when $m_{\max} < 0.2$. The ratio, ϕ, is an insensitive parameter in our model when it is larger than 0.3 (Fig. 5c). Although the water content, ω, in the ice does not directly impact the ice velocity simulations (the flow rate factor A is assumed independent of the water content in ice), the water content can affect the temperature field and, consequently, influence A and the ice velocities (Fig. 5d). From Fig. 6d, we can clearly see that increasing the water content may result in larger TIZ sizes. For example, changing the water content from 1% to 3% nearly doubles the TIZ thickness over a horizontal distance of km 3.5 – 5.8. In addition, we test the sensitivity of the model to different geothermal heat flux values. A larger geothermal heat flux can result in larger TIZs but has a limited impact on ~~modelling~~ modeling ice velocity (Figs. 5e and 6e). As shown by Zhang et al. (2013), our model results are mainly controlled by the shape of the glacial valley, specifically the b index (~~see~~ Sect. 2.1). A large value of b indicates a flat glacial valley and suggests that a small lateral drag was exerted on the ice flow (Figs. 5f and 6f).

Further, we vary the values of c from 0 to 6 K (with a step size of 0.2 K) and compare the modeled 20 m borehole temperatures with *in situ* annual measurements at sites 1 and 2 (Fig. 7). As shown in Fig. 1b, site 1 is located at the center of the confluence area where the convergent flow from the west branch joins the mainstream. Thus, at site 1 it is difficult to find a good c value that predicts close temperature match to the observations (Fig. 7a). We therefore determine the c value (1.6 K) based on the fittings between the modeled and observed ice temperature data at site 2.

Based on the sensitivity experiments described above, we adopt a parameter set of $\lambda_{\text{max}} = 4$ m, $m_{\text{max}} = 0.3$, $\phi = 1$ (no basal water pressure), $\omega = 3\%$, $G = 40$ mW m^{-2}~~and~~, $b = 1.2$, and $c = 1.6$ K as a diagnostic reference in our ~~modelling~~ modeling experiment (E-ref).

4.2 Comparison with *in situ* observations

In the reference experiment (E-ref), we simulate the distributions of horizontal ice velocities and temperatures (Figs. 8a and c). Next, the model results are compared ~~with~~ to the measured ice surface velocities and the ice temperature profile in the deep borehole (Figs. 8b and d). Generally, the ~~modelled~~ modeled ice surface velocities agree well with *in situ* observations from the glacier head to km ~~5.3~~ 4.8 along the CL (Fig. 8b). However, from ~~5.3~~ 4.8 km to the glacier terminus, our model generally underestimates the ice surface ~~velocity because the~~ velocities as shown in all simulations in Fig. 5, which may possibly result from the neglect of the convergent flow from the west branch ~~is ignored~~ and an enhanced basal sliding which is not captured by our model in the confluence area. We verify this hypothesis by conducting two other experiments, E-W and E-WS. In E-W the glacier widths are increased by 450 m at km 5.8 – 7.3 as a proxy of including the impact of the convergent flow from the west branch (Fig. ~~1), as shown in all of the simulations in Fig. 5. The basal sliding velocities are less than 4 m a $^{-1}$ and contribute less than 10~~9). In E-WS, except for the same glacier width increase as in E-W, we also increase λ_{max} by 200% ~~to the mean annual ice surface velocities.~~ and decrease m_{max} by 60% for accelerating the basal sliding at km 5.8 – 7.3 (Fig. 9). We can clearly find that while both factors have a non-negligible contribution to the model results, the basal sliding may play a bit more important role in the confluence area. This indicates a need of considering glacier flow branches and spatially variable sliding law parameters in real glacier modeling studies.

~~We observed~~ The model predicts a TIZ overlain by cold ice over a horizontal distance of km 1.1 – ~~6.5~~ 6.4 (Fig. 8c). In addition, we further validated our numerical model by using *in situ* ~~110m~~ 110 m deep ice temperature measurements (Fig. 8d). In this study, we use a 2D model approach that neglects ice ~~flows~~ fluxes and heat fluxes along the y direction. Consequently, it is very difficult to obtain numerical temperature results that agree perfectly with the *in situ* observations. However, as shown in Fig. 8d, a ~~close~~ match can be found between the model results and *in situ* measurements at depths of approximately 20 – 40 m and 80 – 90 m. The model overestimates the ice temperatures at depths of approximately 50 – 70 m and underestimates the ice temperatures at depths of approximately 100 – 110 m (by less than 0.5 K). Because *in situ* ice temperature data from below 110 m have not been obtained, we were unable to compare the ~~modelled~~ modeled and measured ice temperatures at the ice-bedrock interface.

4.3 Choice of surface thermal boundary condition

We conduct three different numerical experiments (E-air, E-20m, and E-ref) to investigate the impacts of different surface thermal boundary conditions on the thermo-mechanical ~~field~~ fields of LHG12. For the E-air and E-20m experiments, we set $T_{\mathrm{sbc}} = T_{\mathrm{air}}$ and $T_{\mathrm{sbc}} = T_{\mathrm{20m}}$, respectively. E-ref ~~was~~ is adopted in our "real" LHG12 simulations, which uses the ~~T_{20m}~~ $T_{\mathrm{sbc}} = T_{\mathrm{20m}}$ in the accumulation basin and the ~~$(T_{\mathrm{20m}} + T_{\mathrm{air}})/2$~~ $T_{\mathrm{sbc}} = T_{\mathrm{air}} + c$ ($c = 1.6$ K) in the ablation area~~, where the T_{20m} values below the equilibrium line altitude (ELA; approximately 4980 m a. s.l.) are linearly interpolated based on the *in situ* T_{20m} measurements at sites 1 and 2 (Fig. 4).~~ .

The intercomparison results of E-air, E-20m, and E-ref for ice velocities and temperatures are presented in Fig. 10. The ice temperatures along the CL are highly sensitive to T_{sbc}. From E-air, it is observed that LHG12 becomes fully cold, with an average field temperature ~~5.7~~ 5.3 K colder than that of E-ref (Fig. 10a), which decreases the ice surface velocity by approximately ~~13.5~~ 10.0 m a^{-1} (Fig. 10b). Compared with E-ref, E-20m results in larger T_{sbc} values in the ablation area, greater mean ice temperatures (by approximately ~~1.0 K(~~1.5 K; Fig. 10a)~~)~~, greater TIZ thicknesses (by approximately ~~5~~ 9.7 m over a region of km ~~4.0~~ 2.1 – ~~6.0 (~~5.9; Fig. 10c)~~)~~, and faster ice surface velocities (by approximately ~~2~~ 1.5 m a^{-1}~~(~~; Fig. 10b)~~)~~. Next, we compare the ice temperature ~~modelling~~ modeling results with the *in situ* observations of the deep borehole at site 3 (Fig. 10d). E-ref results in the best simulation results, and E-20m, though generally similar to E-ref, generates warmer ice above a depth of 80 m in the deep borehole. Unsurprisingly, E-air results in an unreliable temperature profile that is colder than the actual temperatures at all depths.

As noted ~~in~~ above, the dynamics of LHG12 can be strongly influenced by the choices of different surface thermal boundary conditions. For LHG12, most accumulation and ablation events overlap during the summer season (Sun et al., 2012). The ~~melt-water~~ meltwater entrapped in snow and moulins during the summer season can release large amounts of heat due to refreezing when the temperature decreases, which may significantly increase the ice temperatures in the near-surface snow/ice layers (Fig. 4) and result in the warm bias of T_{20m} (compared with the mean annual surface air temperature). Therefore, compared with E-air, the E-ref and E-20m experiments better incorporate the effects of ~~melt-water~~ meltwater refreezing in the accumulation basin into the prescribed surface thermal boundary constraints resulting in more accurate simulations of ice temperature and flow fields.

4.4 Roles of heat advection, strain heating and basal sliding

To assess the relative contributions of heat advection and strain heating to the thermo-mechanical field of LHG12, we conducted three experiments (E-advZ, E-advX, and E-strain), in which the vertical advection, horizontal along-flow advection and strain heating were ~~"removed"~~neglected, respectively. In addition, to investigate the effects of basal sliding predicted by the Coulomb friction law on the thermal state and flow dynamics of LHG12, we performed an experiment (E-slip) with $u_b = 0$.

~~Fig. ?? compares~~ Figs. 11 and 12 compare the ice velocity and temperature results of E-advZ, E-advX, E-strain and E-slip with those of E-ref. If the vertical advection is ~~"dropped"~~ neglected (E-advZ; cold ice at the glacier surface cannot be transported downwards into the interior of LHG12), LHG12 becomes warmer (Figs. ~~??~~11a and c) and flows faster relative to other experiments (Fig. ~~??~~11b). As described for the discontinuous surface thermal boundary conditions across the ELA (a straightforward result from the refreezing ~~of melt-water~~ meltwater in the accumulation basin), a discontinuous transition of the mean column ice temperature was observed along the CL at km 1.3 (the horizontal position of ELA) in E-advX (Fig. ~~??~~11a). Compared with E-ref, the E-advX experiment predicted colder field temperatures (by approximately ~~2.4~~ 2.7 K) and much smaller surface ice velocities (< ~~18~~ 15.4 m a^{-1}). Because the accumulation basin of LHG12 is relatively warm, E-advX, which ~~"removes"~~ neglects the horizontal transport of ice from upstream and downstream, ~~predicted~~ predicts much colder conditions for LHG12, i.e., the ~~modelled~~ modeled temperate ice only appears at three discontinuous grid points (Fig. ~~??~~11c). As described by Zhang et al. (2015), we observed that strain heating contributes ~~the most~~ greatly to the thermal configuration of LHG12. If we ~~"remove"~~ leave away the strain heating (E-strain), LHG12 becomes fully cold, with a mean ice temperature field lower than that of E-ref by approximately ~~0.85~~ 0.9 K. Consequently, the E-strain experiment predicts lower ice surface velocities (Fig. ~~??~~12b). Previous studies have suggested that basal sliding can significantly influence the thermal structures and velocity fields of glaciers (e.g. Wilson et al., 2013; Zhang et al., 2015). However, in this study the ~~removal~~ neglect of basal sliding (E-slip) results in a temperature field very similar to that of E-ref. We attribute this difference to the relatively small modeled basal sliding values for LHG12. The observed and ~~modelled~~ modeled ice temperature profiles of E-advZ, E-advX, E-strain, E-slip, and E-ref are also compared for the deep ice borehole ~~at site 3 in Fig. ??d .~~ in Figs. 11d and 12d. The differences of the profiles can also be explained by our above explanations.

4.5 Model limitations

Although our 2D, ~~higher-order,~~ first-order, flow-band model can account for part of the three-dimensional nature of LHG12 by parameterizing the lateral drag with glacier width variations, it cannot fully ~~include~~ describe the ice flow ~~and heat advection~~ along the y direction~~. For example, the convergent flow from the west branch could influence the modelled ice velocity from 6.3 km to the glacier terminus (Figs. 5 and 8b).~~ , and are not able to account for the confluence of glacier tributaries. The shape of the LHG12 glacier valley is described using a constant value for index b (1.2; approximately "V" type cross-sections), which was determined from several traverse GPR profiles (Fig. 1). However, for real glaciers, the cross-sectional geometry profiles are generally complex, resulting in an inevitable bias when we idealize the glacier cross-sectional profiles by using power law functions across the entire LHG12 area. Although the regularized Coulomb friction law provides a ~~physically~~ physical relationship between the basal drag and sliding velocities, several parameters (e.g., $\lambda_{\max}$, $m_{\max}$) still must be prescribed based on surface velocity observations. Another uncertainty could be from the spatially uniform geothermal heat flux that we assume in the model, as it may have a great spatial variation due to the mountain topography (Lüthi and Funk, 2001). In addition, we can also improve our model ability by linking the water content in the temperate ice layer to a physical thermo-hydrological process in the future.

Due to the limitations of *in situ* shallow borehole ice temperature measurements, the surface thermal boundary condition in our temperature model is determined using a simple ~~interpolation method~~ parameterization based on observations at three elevations (Fig. 1b). In addition, the ~~method presented by that we follow here for determining the~~ parameterized surface thermal boundary condition only provides a rough estimate of the overall contributions of the heat from refreezing ~~melt-water~~ meltwater and ice flow advection. At this stage, we cannot simulate the actual physical process involved in the transport of near-surface heat from refreezing, which has been suggested by (Gilbert et al., 2012; Wilson and Flowers, 2013). The assumption of steady state neglects the transient effects of past climate and glacier changes, which ~~may have an~~ can have a very important impact on the shape of temperature profile (Lüthi et al., 2015; Gilbert et al., 2015).

5 Conclusions

For the first time, we investigate the thermo-mechanical features of a typical valley glacier, Laohugou Glacier No.12 ~~Glacier~~ (LHG12), ~~on~~ in Mt. Qilian Shan, which is an important fresh water source for the arid regions in western China. We assess the present thermal status of LHG12 using a two-dimensional thermo-mechanically coupled first-order flow-band model using ~~existing *in situ* measurements , e.g.,~~ available *in situ* measurements of glacier geometries, borehole ice temperatures, and surface meteorological and velocity observations. By carefully comparing ~~modelled~~ modeled ice velocities and temperatures with *in situ* observations, we conduct a set of numerical sensitivity experiments that include, for example, basal sliding parameters, geothermal heat fluxes and glacial valley shapes. In addition, we investigate the impacts of different surface thermal conditions (surface air and near-surface ice temperatures), heat advection, strain heating, and basal sliding on our numerical model results.

Similar to other alpine land-terminating glaciers, the mean annual horizontal ice flow speeds ~~(u)~~ of LHG12 are relatively low (less than 40 m a^{-1}). However, we observed large inter-annual variations in the ice surface velocity during the summer and winter seasons. Due to the release of heat from refreezing ~~melt-water~~meltwater, the observed ice temperatures for the shallow ice borehole in the accumulation basin (site 3; Fig. 1) are higher than for the temperatures at sites 1 and 2 at lower elevations, indicating the existence of ~~melt-water~~ meltwater refreezing, as observed in our field expeditions. Thus, we ~~constrain the thermal surface~~ parameterize the surface thermal boundary condition by ~~using the 20m deep ice temperatures~~ accounting for the 20 m deep temperature instead of only the surface air temperatures. We observed that LHG12 has a polythermal structure with a temperate ice zone ~~(approximately 5.4 km long)~~ that is overlain by cold ice near the glacier base throughout a large region of the ablation area.

Horizontal heat advection is important on LHG12 for bringing the relatively warm ice in the accumulation basin (due to the heat from refreezing ~~melt-water~~meltwater) to the downstream ablation zone. In addition, vertical heat advection is important for transporting the near-surface cold ice downwards into the glacier interior, which "cools down" the ice temperature. Furthermore, we argue that the strain heating of LHG12 ~~plays the most~~ also plays an important role in controlling the ~~en-glacial~~ englacial thermal status, as suggested by Zhang et al. (2015). However, we also observed that simulated basal sliding contributes little to the thermal-mechanical configuration of LHG12 (very small; < 4 m a^{-1}).

The mean annual surface air temperature could serve as a good approximation for the temperatures of shallow ice, where seasonal climate variations are damped at cold and dry locations (Cuffey and Paterson, 2010). However, for LHG12, using the mean annual surface air temperature as the thermal boundary condition at the ice surface would predict an entirely cold glacier with very small ice flow speeds. Because warming is occurring on alpine glaciers in, for example, Mt. Himalayas and Qilian

Shan, further studies of supra-glacial and near-surface heat transport are very important because they will affect the surface thermal conditions and, eventually, the dynamical behaviours of the glacier.

Acknowledgements. This work is supported by the National Basic Research Program (973) of China (2013CBA01801, 2013CBA01804), and the Technology Services Network Program (STS-HHS Program) of Cold and Arid Regions Environmental and Engineering Research Institute, Chinese Academy of Sciences (HHS-TSS-STS-1501). We are grateful to numerous people for their hard fieldwork. We thank the supports from the Qilian Shan Station of Glaciology and Ecologic Environment, Chinese Academy of Sciences (CAS). We thank Martin Lüthi and an anonymous reviewer for their thorough and constructive reviews which significantly improved the manuscript.

References

Blatter, H. and Greve, R.: Comparison and verification of enthalpy schemes for polythermal glaciers and ice sheets with a one-dimensional model, Polar Science, 9, 196–207, 2015.

Blatter, H. and Hutter, K.: Polythermal conditions in Arctic glaciers, Journal of Glaciology, 37, 261–269, 1991.

Cuffey, K. and Paterson, W.: The Physics of Glaciers, Elsevier, Amsterdam, 4^{th} edn., 2010.

De Smedt, B., Pattyn, F., and De Groen, P.: Using the unstable manifold correction in a Picard iteration to solve the velocity field in higher-order ice-flow models, Journal of Glaciology, 56, 257–261, 2010.

Du, W., Qin, X., Liu, Y., and Wang, X.: Variation of the Laohugou Glacier No.12 in the Qilian Mountains. (in Chinese with English summary), Journal of Glaciology and Geocryology, 30, 373–379, 2008.

Flowers, G. E., Roux, N., Pimentel, S., and Schoof, C. G.: Present dynamics and future prognosis of a slowly surging glacier, The Cryosphere, 5, 299–313, 2011.

Funk, M., Echelmeyer, K. A., and Iken, A.: Mechanisms of fast flow in Jakobshavn Isbræ, West Greenland: Part II. Modeling of englacial temperatures, Journal of Glaciology, 40, 569–585, 1994.

Gagliardini, O., Cohen, D., Råback, P., and Zwinger, T.: Finite-element modeling of subglacial cavities and related friction law, Journal of Geophysical Research, 112, F02 027, 2007.

Gilbert, A., Wagnon, P., Vincent, C., Ginot, P., and Funk, M.: Atmospheric warming at a high-elevation tropical site revealed by englacial temperatures at Illimani, Bolivia (6340 m above sea level, 16°S, 67°W), Journal of Geophysical Research, 115, D10 109, 2010.

Gilbert, A., Vincent, C., Wagnon, P., Thibert, E., and Rabatel, A.: The influence of snow cover thickness on the thermal regime of Tête Rousse Glacier (Mont Blanc range, 3200 m a.s.l.): Consequences for outburst flood hazards and glacier response to climate change, Journal of Geophysical Research, 117, 2012.

Gilbert, A., Gagliardini, O., Vincent, C., and Wagnon, P.: A 3-D thermal regime model suitable for cold accumulation zones of polythermal mountain glaciers, Journal of Geophysical Research: Earth Surface, 119, 1876–1893, 2014a.

Gilbert, A., Vincent, C., Six, D., Wagnon, P., Piard, L., and Ginot, P.: Modeling near-surface firn temperature in a cold accumulation zone (Col du Dôme, French Alps): from a physical to a semi-parameterized approach, The Cryosphere, 8, 689–703, 2014b.

Gilbert, A., Vincent, C., Gagliardini, O., Krug, J., and Berthier, E.: Assessment of thermal change in cold avalanching glaciers in relation to climate warming, Geophysical Research Letters, 42, 6382–6390, 2015.

Guo, W., Xu, J., Liu, S., Shangguan, D., Wu, L., Yao, X., Zhao, J., Liu, Q., Jiang, Z., Li, P., Wei, J., Bao, W., Yu, P., Ding, L., Li, G., Ge, C., and Wang, Y.: The second glacier inventory dataset of China (Version 1.0), Cold and Arid Regions Science Data Center at Lanzhou, 2014.

Guo, W., Liu, S., Xu, J., Wu, L., Shangguan, D., Yao, X., Wei, J., Bao, W., Yu, P., Liu, Q., and Jiang, Z.: The second Chinese glacier inventory: data, methods and results, Journal of Glaciology, 61, 357–372, 2015.

Huang, M.: On the temperature distribution of glaciers in China, Journal of Glaciology, 36, 210–216, 1990.

Huang, M.: Forty year's study of glacier temperature in China. (in Chinese with English summary), Journal of Glaciology and Geocryology, 21, 193–199, 1999.

Huang, M., Wang, Z., and Ren, J.: On the temperature regime of continental-type glaciers in China, Journal of Glaciology, 28, 117–128, 1982.

Huss, M., Jouvet, G., Farinotti, D., and Bauder, A.: Future high-mountain hydrology: a new parameterization of glacier retreat, Hydrology and Earth System Sciences, 14, 815–829, 2010.

Irvine-Fynn, T. D. L., Hodson, A. J., Moorman, B. J., Vatne, G., and Hubbard, A. L.: Polythermal glacier hydrology: A review, Reviews of Geophysics, 49, 2011.

Jansson, P., Hock, R., and Schneider, T.: The concept of glacier storage: a review, Journal of Hydrology, 282, 116–129, 2003.

Liu, Y., Hou, S., Wang, Y., and Song, L.: Distribution of borehole temperature at four high-altitude alpine glaciers in Central Asia, Journal of Mountain Science, 6, 221–227, 2009.

Liu, Y., Qin, X., Du, W., Sun, W., and Hou, D.: The movement features analysis of Laohugou Glacier No.12 in Qilian Mountains, Sciences in Cold and Arid Regions, 3, 119–123, 2011.

Lüthi, M. P. and Funk, M.: Modelling heat flow in a cold, high-altitude glacier: interpretation of measurements from Colle Gnifetti, Swiss Alps, Journal of Glaciology, 47, 314–324, 2001.

Lüthi, M. P., Ryser, C., Andrews, L. C., Catania, G. A., Funk, M., Hawley, R. L., Hoffman, M. J., and Neumann, T. A.: Heat sources within the Greenland Ice Sheet: dissipation, temperate paleo-firn and cryo-hydrologic warming, The Cryosphere, 9, 245–253, 2015.

Meierbachtol, T. W., Harper, J. T., Johnson, J. V., Humphrey, N. F., and Brinkerhoff, D. J.: Thermal boundary conditions on western Greenland: Observational constraints and impacts on the modeled thermomechanical state, Journal of Geophysical Research: Earth Surface, 120, 623–636, 2015.

Neckel, N., Kropáček, J., Bolch, T., and Hochschild, V.: Glacier mass changes on the Tibetan Plateau 2003–2009 derived from ICESat laser altimetry measurements, Environmental research letters, 9, 014 009, 2014.

Pattyn, F.: Transient glacier response with a higher-order numerical ice-flow model, Journal of Glaciology, 48, 467–477, 2002.

Schäfer, M., Gillet-Chaulet, F., Gladstone, R., Pettersson, R., A. Pohjola, V., Strozzi, T., and Zwinger, T.: Assessment of heat sources on the control of fast flow of Vestfonna ice cap, Svalbard, The Cryosphere, 8, 1951–1973, 2014.

Schoof, C.: The effect of cavitation on glacier sliding, Royal Society of London Proceedings Series A, 461, 609–627, 2005.

Shi, Y. and Liu, S.: Estimation on the response of glaciers in China to the global warming in the 21st century, Chinese Science Bulletin, 45, 668–672, 2000.

Sugiyama, S., Sakakibara, D., Matsuno, S., Yamaguchi, S., Matoba, S., and Aoki, T.: Initial field observations on Qaanaaq ice cap, northwestern Greenland, Annals of Glaciology, 55, 25–33, 2014.

Sun, W., Qin, X., Ren, J., Yang, X., Zhang, T., Liu, Y., Cui, X., and Du, W.: The surface energy budget in the accumulation zone of the Laohugou Glacier No.12 in the western Qilian Mountains, China, in summer 2009, Arctic, Antarctic, and Alpine Research, 44, 296–305, 2012.

Svensson, H.: Is the cross-section of a glacial valley a parabola?, Journal of Glaciology, 3, 362–363, 1959.

Tian, H., Yang, T., and Liu, Q.: Climate change and glacier area shrinkage in the Qilian Mountains, China, from 1956 to 2010, Annals of Glaciology, 55, 187–197, 2014.

Van der Veen, C. J.: A numerical scheme for calculating stresses and strain rates in glaciers, Mathematical geology, 21, 363–377, 1989.

Vincent, C., Le Meur, E., Six, D., Possenti, P., Lefebvre, E., and Funk, M.: Climate warming revealed by englacial temperatures at Col du Dôme (4250 m, Mont Blanc area), Geophysical Research Letters, 34, L16 502, 2007.

Wang, Y., Ren, J., Qin, X., Liu, Y., Zhang, T., Chen, J., Li, Y., and Qin, D.: Ice depth and glacier-bed characteristics of Laohugou Glacier No.12, Qilian Mountains, revealed by ground-penetrating radar. (in Chinese with English summary), Journal of Glaciology and Geocryology, 1, 28–35, 2016.

Wilson, N. J. and Flowers, G. E.: Environmental controls on the thermal structure of alpine glaciers, The Cryosphere, 7, 167–182, 2013.

Wilson, N. J., Flowers, G. E., and Mingo, L.: Comparison of thermal structure and evolution between neighboring subarctic glaciers, Journal of Geophysical Research: Earth Surface, 118, 1443–1459, 2013.

Yao, T., Thompson, L., Yang, W., Yu, W., Gao, Y., Guo, X., Yang, X., Duan, K., Zhao, H., and Xu, B.: Different glacier status with atmospheric circulations in Tibetan Plateau and surroundings, Nature Climate Change, 2, 663–667, 2012.

Zhang, T., Xiao, C., Colgan, W., Qin, X., Du, W., Sun, W., Liu, Y., and Ding, M.: Observed and modelled ice temperature and velocity along the main flowline of East Rongbuk Glacier, Qomolangma (Mount Everest), Himalaya, Journal of Glaciology, 59, 438–448, 2013.

Zhang, T., Ju, L., Leng, W., Price, S., and Gunzburger, M.: Thermomechanically coupled modelling for land-terminating glaciers: a comparison of two-dimensional, first-order and three-dimensional, full-Stokes approaches, Journal of Glaciology, 61, 702–712, 2015.

Table 1. Parameters used in this study

Symbol	Description	Value	Unit
β	Clausius-Clapeyron constant	8.7×10^{-4}	K m^{-1}
g	Gravitational acceleration	9.81	m s^{-2}
ρ	Ice density	910	kg m^{-3}
ρ_{w}	Water density	1000	kg m^{-3}
n	Exponent in Glen's flow law	3	-
$\dot{\epsilon}_0$	viscosity regularization	10^{-30}	a^{-1}
A_0	Flow law parameter		
	when T ≤ 263.15 K	3.985×10^{-13}	Pa^{-3} s^{-1}
	when T > 263.15 K	1.916×10^{3}	Pa^{-3} s^{-1}
Q	Creep activation energy		
	when T ≤ 263.15 K	60	kJ mol^{-1}
	when T > 263.15 K	139	kJ mol^{-1}
R	Universal gas constant	8.31	J mol^{-1} K^{-1}
k	Thermal conductivity	2.1	W m^{-1} K^{-1}
c_p	Heat capacity of ice	2009	J kg^{-1} K^{-1}
L	Latent heat of fusion of ice	3.35×10^{-5}	J kg^{-1}
T_0	Triple-point temperature of water	273.16	K

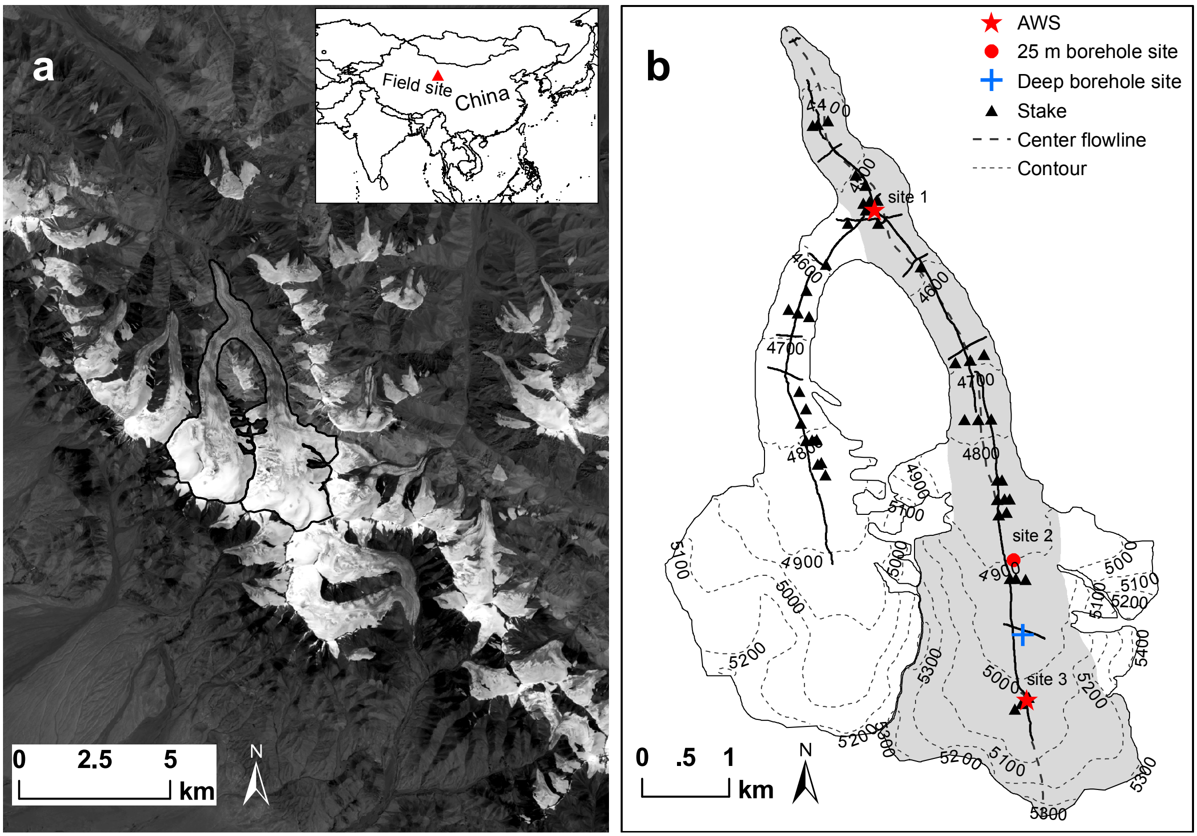

Figure 1. ~~Map~~ (a) The location of LHG12 in the west Mt. Qilian Shan, China. (b) The solid and thick black lines indicate the GPR survey lines. The shaded area denotes the mainstream of LHG12, which only includes the east branch and neglects the west branch and all small tributaries. The dashed black line represents the center ~~flow-line~~flowline. Red stars indicate the locations of the automatic weather stations and the ~~25m~~ 25 m deep shallow boreholes (sites 1 and 3). A solid red circle represents the location of the shallow borehole at site 2, and a blue cross represents the location of the deep ice borehole. Black triangles show the positions of the stakes used for ice surface velocity measurements. The contours were generated from SRTM DEM in 2000.

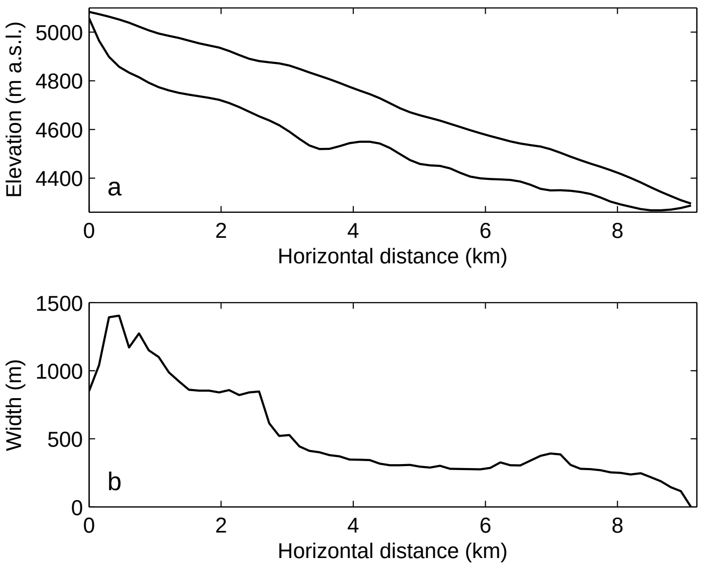

Figure 2. (a) Glacier surface and bed topography along the center ~~flow-line~~flowline. (b) Glacier widths along the center ~~flow-line~~flowline.

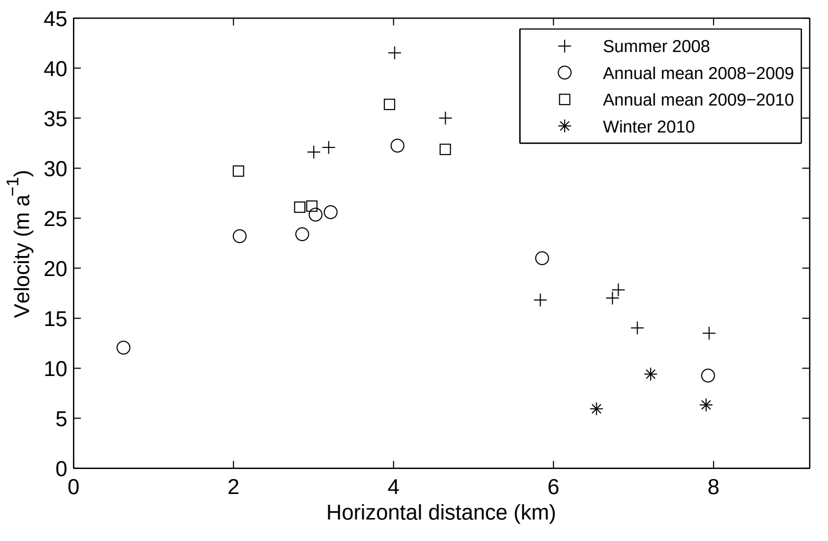

Figure 3. Measured ice surface velocities along the center ~~flow-line~~flowline.

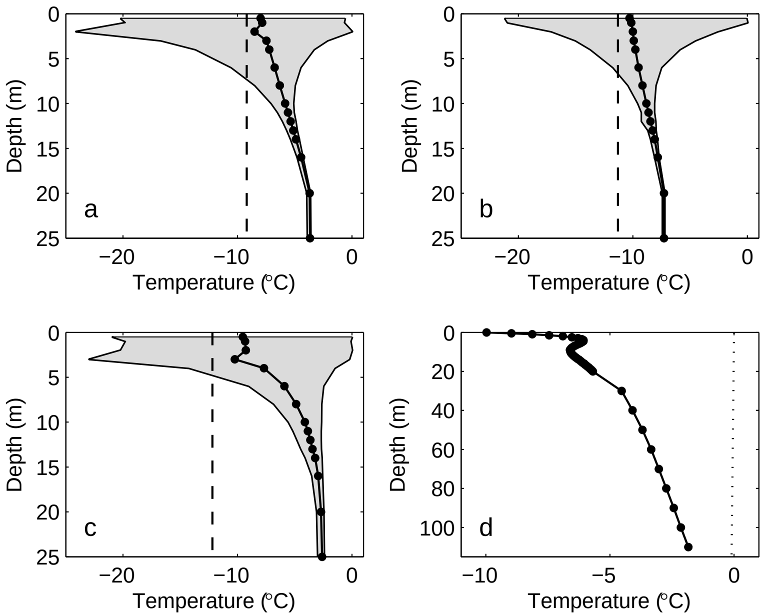

Figure 4. Ice temperature measurements from the four ice boreholes. (a, b, c) Ice temperature measurements from the ~~25m~~ 25 m deep boreholes at sites 1, 2, and 3, respectively. The black dots show the mean annual ice temperatures over the period of 2010 – 2011. The shaded areas show the yearly fluctuation range of the ice temperature. The dashed lines indicate the mean annual air temperature. (d) Measured ice temperatures from the deep borehole. The dotted line denotes the pressure-melting point (PMP) as a function of elevation.

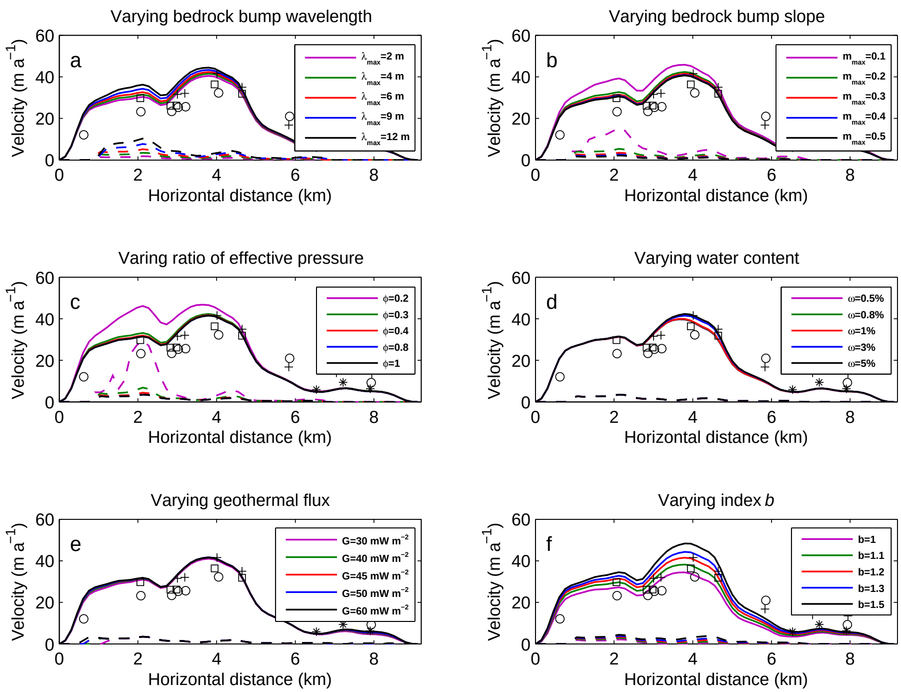

Figure 5. The sensitivity of the ~~modelled~~ modeled ice flow speeds to parameters along the CL. The solid and dashed lines indicate the ~~modelled~~ modeled surface and basal sliding velocities, respectively. Symbols show the measured ice surface velocities (~~see~~ Fig. 3).

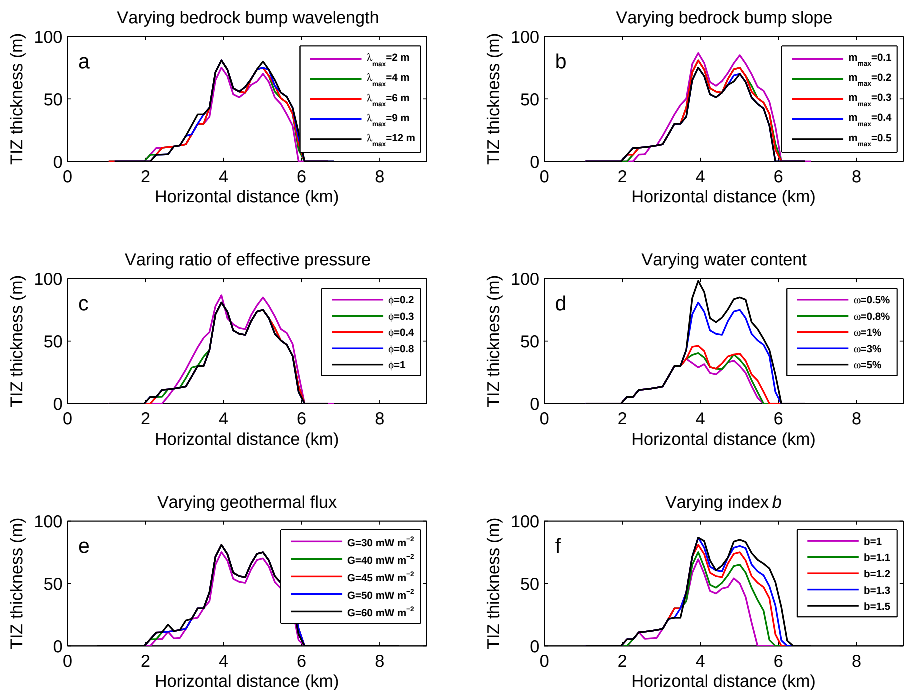

Figure 6. The sensitivity of the ~~modelled~~ modeled temperate ice thicknesses to parameters along the CL. The parameter settings are same as those described in Fig. 5.

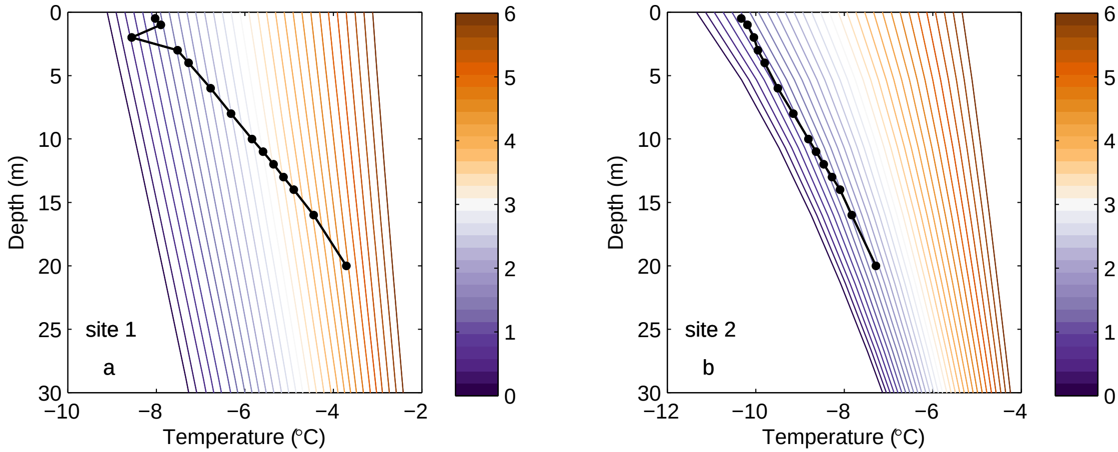

Figure 7. ~~A comparison~~ Sensicitity experiments of the ~~modelled and~~ tuning parameter c by comparing the measured ~~ice temperatures and horizontal velocities~~ (~~u~~black dotted lines) ~~. (a) The distribution of the modelled horizontal ice velocity (u). (b) Measured (symbols)~~ and ~~modelled~~ modeled (~~solid line~~coloured lines) ~~surface and basal (dashed line) horizontal velocities. The symbols are the same as described in Fig. 3. (c) The distribution of the modelled ice temperature. The blue dashed line indicates the CTS position, and the black bar shows the location of the deep ice~~ 20 m borehole ~~.~~ temperatures at sites 1 (~~d~~a) ~~Modeled (blue line)~~ and ~~measured~~ 2 (~~dots~~b)~~ice temperature profiles for the deep borehole~~. The ~~pressure-melting point is shown by~~ step size of varying the ~~dotted line~~c value is 0.2 K.

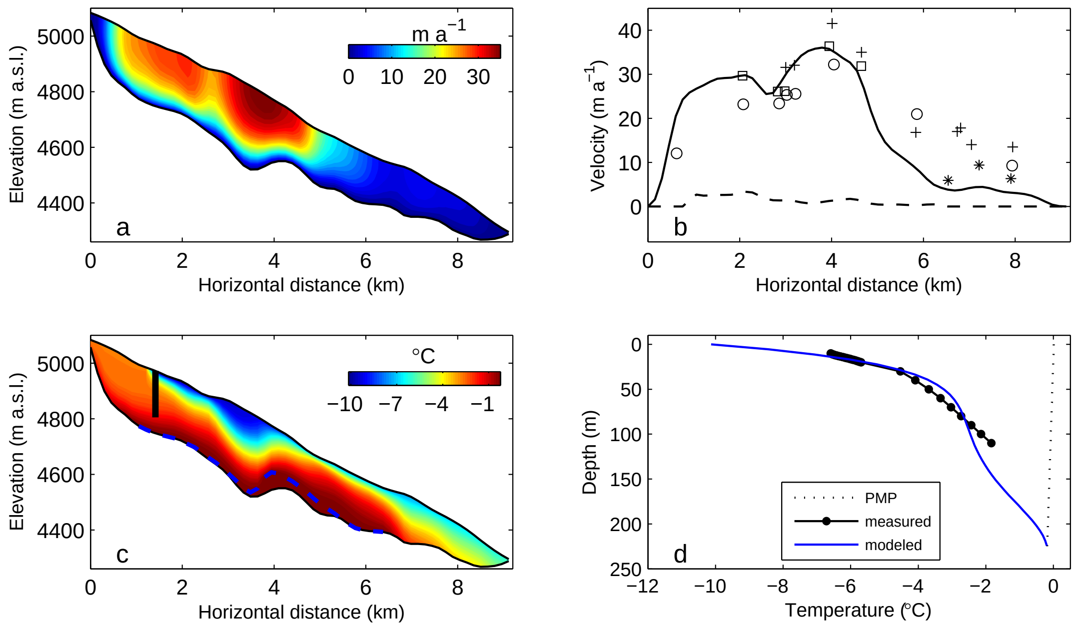

Figure 8. A comparison of the modeled and measured ice temperatures and horizontal velocities (u). (a) The distribution of the modeled horizontal ice velocity (u). (b) Measured (symbols) and modeled (solid line) surface and basal (dashed line) horizontal velocities. The symbols are the same as described in Fig. 3. (c) The distribution of the modeled ice temperature. The blue dashed line indicates the CTS position, and the black bar shows the location of the deep ice borehole. (d) Modeled (blue line) and measured (dots) ice temperature profiles for the deep borehole. The pressure-melting point is shown by the dotted line.

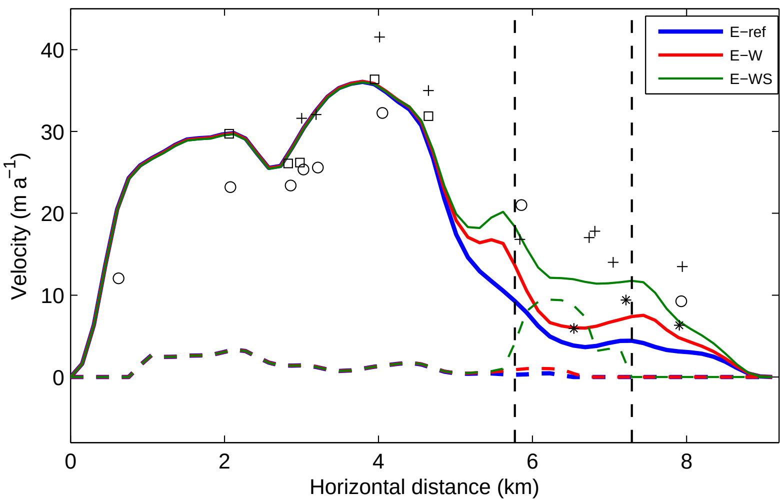

Figure 9. Modeled ice ~~temperatures and~~ velocities for experiments E-ref (blue line), ~~E-air~~ E-W (red line), and ~~E-20m~~ E-WS (green line). ~~(a) Modeled column mean (solid lines) and basal (dashed lines) ice temperatures along the CL. (b) Modeled surface (solid lines) and basal (dashed lines) ice velocities along the CL.~~ The ~~symbols for the measured ice surface velocities are the same as those shown~~ glacier widths in ~~Fig. 3. (c) Modeled CTS position. The black bar shows~~ the ~~location~~ zone of ~~the deep ice borehole.~~ km 5.8 – 7.3 (~~d) Measured (coloured~~ bounded by the vertical dashed lines) ~~and modelled (dots) ice temperature profiles~~ are increased by 450 m for ~~the deep borehole~~E-W and E-WS. ~~The dotted line shows the pressure-melting point as~~ In E-WS we also include a ~~function of ice depth~~basal sliding enhancement between km 5.8 – 7.3.

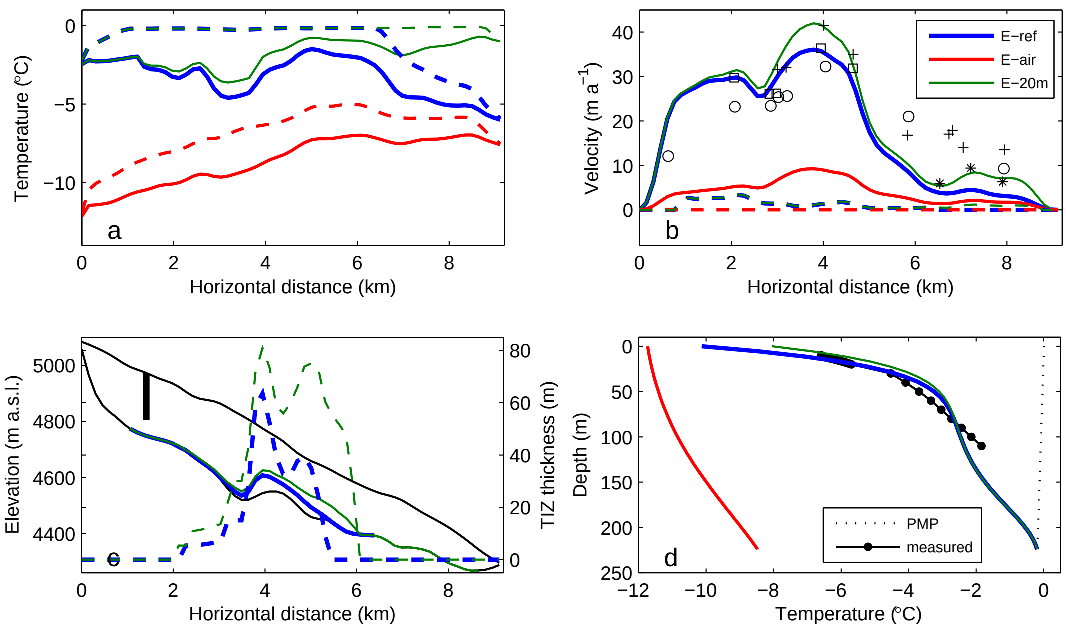

Figure 10. Modeled ice temperatures and velocities for experiments E-ref (blue line), E-air (red line), and E-20m (green line). (a) Modeled column mean (solid lines) and basal (dashed lines) ice temperatures along the CL. (b) Modeled surface (solid lines) and basal (dashed lines) ice velocities along the CL. The symbols for the measured ice surface velocities are the same as those shown in Fig. 3. (c) Modeled CTS position (solid lines) and TIZ thickness (dashed lines). The black bar shows the location of the deep ice borehole. (d) Measured (dots) and modeled (coloured lines) ice temperature profiles for the deep borehole. The dotted line shows the pressure-melting point as a function of ice depth.

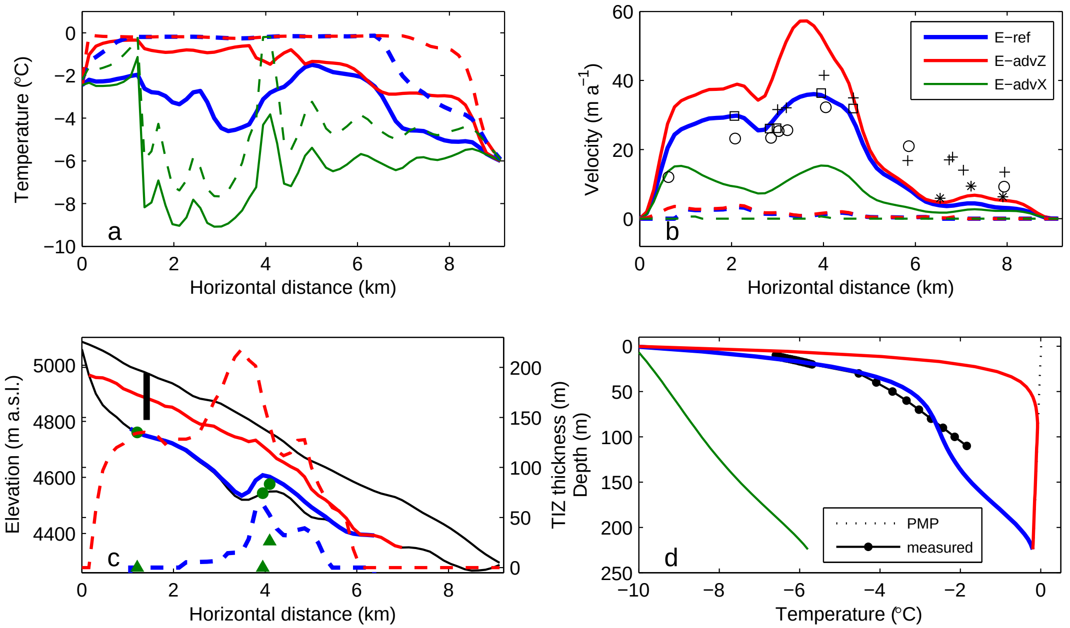

Figure 11. Modeled ice temperatures and velocities for experiments E-ref (blue line), E-advZ (red line) ~~,~~ and E-advX (green line)~~, E-strain (purple line), and E-slip (yellow line)~~. (a) Modeled column mean (solid lines) and basal (dashed lines) ice temperatures along the CL. (b) Modeled surface (solid lines) and basal (dashed lines) ice velocities along the CL. The symbols for the measured ice surface velocities are the same as those shown in Fig. 3. (c) Modeled CTS position (solid lines and filled circles) and TIZ thickness (dashed lines and filled triangles). The filled circles and triangles denote the discontinuous CTS locations and TIZ thicknesses in E-advX, respectively. The black bar shows the location of the deep ice borehole. (d) Measured (~~coloured lines~~dots) and ~~modelled~~ modeled (~~dots~~coloured lines) ice temperature profiles for the deep borehole. The dotted line shows the pressure-melting point as a function of ice depth.

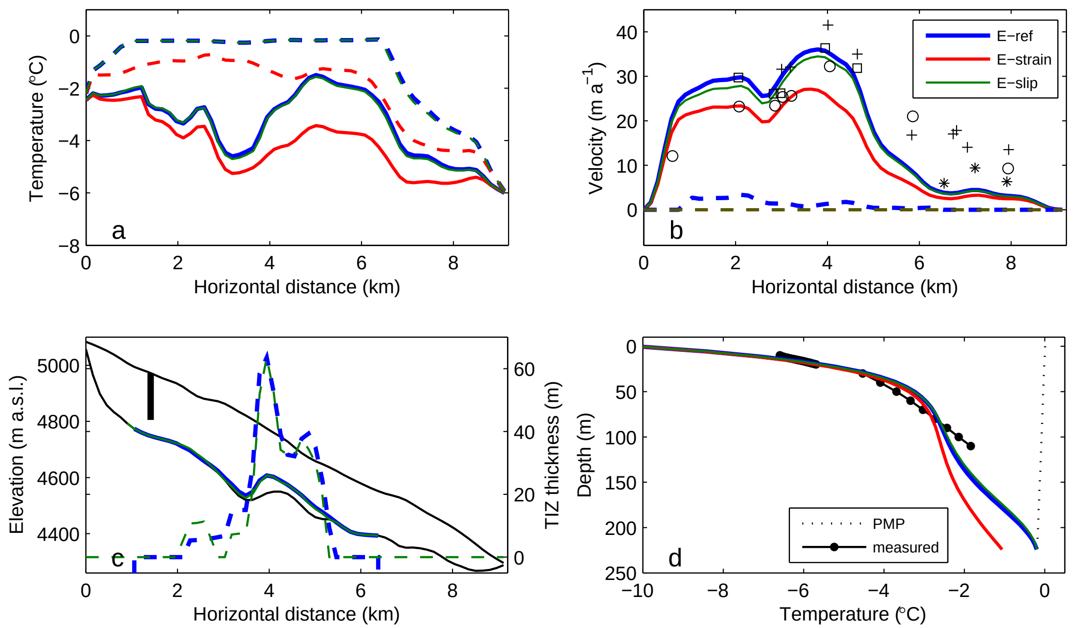

Figure 12. Modeled ice temperatures and velocities for experiments E-ref (blue line), E-strain (green line) and E-slip (purple line). (a) Modeled column mean (solid lines) and basal (dashed lines) ice temperatures along the CL. (b) Modeled surface (solid lines) and basal (dashed lines) ice velocities along the CL. The symbols for the measured ice surface velocities are the same as those shown in Fig. 3. (c) Modeled CTS position (solid lines) and TIZ thickness (dashed lines). The black bar shows the location of the deep ice borehole. (d) Measured (dots) and modeled (coloured lines) ice temperature profiles for the deep borehole. The dotted line shows the pressure-melting point as a function of ice depth.